THE ASTROPHYSICAL JOURNAL, 409:429–449, 1993 May 20

EQUATORIAL DISK FORMATION AROUND ROTATING STARS DUE TO RAM PRESSURE CONFINEMENT BY THE STELLAR WIND

J. E. BJORKMAN AND J. P. CASSINELLI
Department of Astronomy, University of Wisconsin, 475 North Charter Street, Madison, WI 53706
Received 1992 April 13; accepted 1992 November 13

ABSTRACT

We present a simple approximation that permits us to obtain the axisymmetric two-dimensional supersonic solution of a rotating radiation-driven stellar wind from the Friend & Abbott one-dimensional model of the equatorial flow. Our solution predicts the formation of a dense equatorial disk if the rotation rate of the star is above a threshold value, which depends on the ratio of the terminal speed of the wind to the escape speed of the star.

Along the upper main sequence (earlier than B2), both the observed and theoretical values for this ratio decrease monotonically toward later spectral types. For early O stars, the disk can only form if the rotation speed is in excess of 90% of the critical (breakup) speed. For B2 stars, the disk forms at rotation speeds above 50%–60% of the critical rotation speed, depending on the adopted terminal speed (observational vs. theoretical estimates). This corresponds to a rotation speed $V_{\rm rot} > 230$–300 km s^{-1}. Later than B2, the theoretical terminal speed ratio increases, and at B9 the disk forms when the rotation speed exceeds 73% of the critical value. The change in the disk formation threshold as a function of spectral type qualitatively explains the frequency distribution of Be stars and indicates a maximum probability around B2.

The disk is formed because the supersonic wind that leaves the stellar surface at high latitudes travels along trajectories that carry it down to the equatorial plane, where the material passes through a standing oblique shock on top of the disk. The ram pressure of the polar wind thus confines and compresses the disk. For Be stars, the disk is predicted to be quite thin ($\approx 0.^\circ 5$ opening angle) and has a density enhancement $\rho_{\rm eq}/\rho_{\rm pole} \approx 10^3$. This compression is large enough to potentially explain the discrepancy between the inferred UV and IR mass-loss rates of Be stars. Adjacent to the disk, the standing shock heats the flow that enters the equatorial region to temperatures of 10^5–10^6 K before the material finally mixes with the disk. This temperature is sufficient to produce superionization in the winds of Be stars, and the shock location explains observations indicating that C IV is concentrated toward the equator. In addition, the shock temperature indicates that Be stars will be EUV and soft X-ray emitters.

Subject headings: stars: circumstellar matter — stars: early type — stars: emission-line, Be — stars: mass loss — stars: rotation

1. INTRODUCTION

Hot stars have radiatively driven stellar winds, which can produce a relatively dense radiatively ionized circumstellar envelope. At short wavelengths (typically UV), the spectral lines often exhibit redshifted emission and blueshifted absorption (P Cygni line profiles), which is evidence of high-velocity outflow from the star. At long wavelengths (typically far-IR and radio), the envelope is optically thick, and free-free emission produces excess radiation in the stellar spectrum. In some cases, the envelope is not spherically symmetric; consequently, electron scattering produces intrinsic polarization of the stellar spectrum. In particular, three classes of hot stars, Be, Wolf-Rayet, and B[e], all exhibit optical polarization (Coyne & McLean 1982; Schmidt 1988; Schulte-Ladbeck & Zickgraf 1988). On average, Be stars have higher $v \sin i$ values than normal B stars (Slettebak 1982), and it is commonly believed that the rapid rotation is the cause of the inferred asymmetries in Be star envelopes. It has also been suggested that B[e] and Wolf-Rayet stars are rapid rotators as well (Zickgraf et al. 1986; Poe, Friend, & Cassinelli 1989; Cassinelli et al. 1989). Empirical modeling of each of these three classes of stars has led to a two-component picture for the structure of their envelopes: a slow dense equatorial disk component, and a fast tenuous polar component over the remainder of the star. The polar component is consistent with a radiation-driven wind; however, the origin of the disk component is especially uncertain, and it is this problem that is the focus of this paper.

1.1. *Observational Background*

The two-component picture of the extended atmosphere around Be stars has been derived from observations over a broad range of the spectrum. In the optical, a classical Be star exhibits variable hydrogen Balmer emission lines (and often times Fe II) with widths of a few hundred km s^{-1}. Many Be spectra possess narrow absorption "shell" features in the spectral lines of the lower ionization stages. The Be stars are also found to have surprisingly large excess continuum radiation, due to free-free emission, in the near-IR (Gehrz, Hackwell, & Jones 1974), far IR (from *IRAS* data, Coté & Waters 1987) and radio (Taylor et al. 1987). Combining all of these observations, one is led to the conclusion that there is a dense, low-velocity, low-ionization stage component in the circumstellar envelope. There is a good correlation between the IR excess, measured at 12 μm, and the optical polarization (Coté & Waters 1987), which indicates that this dense component is not spherically symmetric. Since these stars are rapidly rotating, it is reasonable to suppose that this material is contained in an equatorial disk. In support of the disk hypothesis are the observations of Be/X-ray binaries—the most common class of luminous X-ray binaries among hot stars. The X-rays appear in one or two

bursts per orbital period. This is consistent with the enhanced accretion onto the neutron star companion that results from its passage through the dense equatorial disk of the Be star (for a review see van den Heuvel & Rappaport 1987).

Many empirical models of Be star disks have been developed to interpret these observations (e.g., Pockert & Marlborough 1976). In particular, by modeling the IR excess versus wavelength, Waters (1986) and Waters, Coté, & Lamers (1987) have estimated the density structure for a number of Be star disks. At the base of the disk (i.e., near the stellar surface), they obtain a disk density, ρ_0, on the order of 10^{-12} to 10^{-11} g cm^{-3}. By combining this model with the X-ray binary data, the terminal velocity in the disk may be determined, since the X-ray luminosity depends, via the accretion rate, on the density and flow speed in the disk. For most cases, this indicates an equatorial outflow of 100–300 km s^{-1} (Waters et al. 1988; Waters 1989).

In addition to the disk, Be stars also have stellar winds with speeds $\approx 10^3$ km s^{-1}, which are detected by the presence of asymmetric blueshifted absorption in the ultraviolet resonance lines of C IV (1550 Å) and Si IV (1400 Å). The UV lines, as analyzed by Snow (1981), indicate a mass-loss rate of about 10^{-11} to 10^{-9} $M_\odot$ yr^{-1}. A plot of the UV mass-loss rate versus luminosity (Snow 1982) shows a strong power-law dependence that is nearly an extrapolation of the law obeyed by the more luminous O and OB supergiant stars, and is in rough agreement with the theoretical mass-loss rate derived by Castor, Abbott, & Klein (1975, hereafter CAK). This leads to the suggestion that the UV line-producing portion of the wind is radiatively driven in Be stars.

One of the most peculiar properties of Be stars is that the mass-loss rate derived from the IR excess is a factor of 10^2–10^4 times larger than that derived from the UV (Waters et al. 1987), and shows a much weaker dependence on stellar luminosity. In addition, Hα line widths are on the order of a few hundred km s^{-1}; whereas, the UV edge velocities are about 1000 km s^{-1}. It is this disparity between the UV, IR, and optical results that has led to the two-component picture for the outer envelope of Be stars in which one component is a high-speed, highly ionized, low-density, radiatively driven outflow in the polar regions, and the second component is a low-speed, weakly ionized, high-density outflow in the equatorial disk. In this picture, the UV resonance lines are formed in the polar component, and the IR excess and Hα emission are formed in the disk component. The optical polarization then results from scattering by the asymmetric distribution of electrons.

As noted previously, this picture is not unique to Be stars, which are of luminosity classes III through V. The much more luminous B[e] stars (sometimes called Be supergiants) also show evidence for a two-component wind (Zickgraf et al. 1986). This two-component model has also been applied to Wolf-Rayet stars to explain the wind momentum problem of these objects (Poe et al. 1989).

In apparent contradiction to the two-component model of Be star envelopes is the evidence of a connection between the equatorial and polar components. In studies of the time variability of 59 Cyg, the C IV line, which is a "superionized" state in Be stars (higher stage of ionization than would be expected for that spectral type), was seen to vary in conjunction with changes in the Hα equivalent width, as well as with variations in the V/R ratio (Doazan et al. 1985). This indicates that the superionization and the equatorial disk are somehow linked. In support of this, K. S. Bjorkman (1989) and Grady, Bjorkman, & Snow (1987) and Grady et al. (1989) have found statistical trends in the C IV equivalent widths, edge velocities, and presence of discrete absorption components verses inclination angle and $v \sin i$ that are consistent with an equatorial concentration of C IV rather than a polar concentration. This has been quite puzzling, since these results imply that, somehow, the high-velocity superionized region exists at the same latitude as the low-ionization-stage, low-velocity equatorial disk.

Superionization can be explained as a result of either collisional ionization in a gas with temperatures higher than 10^5 K, or radiative ionization by the Auger process following K-shell absorption of X-rays in the envelope (Cassinelli & Olson 1979). Either of these processes indicate temperatures far in excess of the radiative equilibrium temperature around the star. One mechanism for producing such temperatures is shock heating of the material. Since the superionization appears to be linked to the disk, one may speculate that somehow shocks play a role in the formation of the disk.

1.2. *Theoretical Background*

All of the above properties form pieces of what is generally called the "Be phenomenon." There is, as yet, no theoretical model that can simultaneously account for all the phenomena. Clearly rotation is involved, as is a mechanism for driving a stellar wind. Previous models of the wind from a rotating star have mostly been one-dimensional models of the equatorial flow versus the polar flow, although one two-dimensional numerical calculation has been performed by Poe (1987). The one-dimensional models of Friend & Abbott (1986, hereafter FA) and Pauldrach, Puls, & Kudritzki (1986) examined the equatorial flow using the CAK form for the radiation forces, and they also included the correction for the finite angular size of the stellar disk. However, the resulting mass-loss rates are insufficient to produce the large densities and low velocities required to match the observations of Be stars. To increase the equatorial mass-loss rate, it was believed that additional forces must play a role.

Friend & MacGregor (1984) examined the effect of adding the Lorentz forces resulting from a rotating stellar magnetic field. They generalized the Weber & Davis (1967) magnetically driven wind to include radiation pressure resulting from line opacity. Poe & Friend (1986) extended this model to include the effects of the finite size of the stellar disk, and they derived the properties of the outflow in the equatorial zone of a rapidly rotating B star. With a rotation rate of 87% of the critical value, which is higher than is typically observed in Be stars, the Poe & Friend model can only produce a density contrast of about a factor of 5 from equator to pole. It cannot explain the Be phenomena, because the equatorial wind speed is too large ($\approx 10^3$ km s^{-1} instead of the observed 10^2 km s^{-1}) and the density in the equator is an order of magnitude too small.

A mechanism that does produce a slow dense wind is the bi-stability of radiation-driven winds, which was discovered by Pauldrach & Puls (1990) in their study of the slow massive wind from the hypergiant P Cygni (B1 Ia$^+$). This star has a mass-loss rate of about 10^{-5} $M_\odot$ yr^{-1}, which is not unusual for such a very luminous star; however, the terminal velocity of the star is only about 200 km s^{-1}. In contrast, supergiants of the same spectral class usually have winds with speeds of greater than 1000 km s^{-1}. Pauldrach & Puls found that, for a star with a temperature of 15–18 $\times$ 10^3 K, if the mass-loss rate is large enough to be optically thick in the Lyman continuum (they vary the surface gravity to achieve this), then the wind shifts to a lower ionization state and the dominant driving lines

for the wind shift from being the strong EUV resonance lines to being the weaker but more numerous iron lines in the Balmer continuum. The wind that is driven by these lines is slow—in agreement with the P Cygni wind.

Recently, Lamers & Pauldrach (1991) suggested that this bi-stability could be operating in the winds of rapidly rotating stars with temperatures like those of P Cygni, such as Be and B[e] stars. Suppose that in the polar region of a rapidly rotating star, where the ionizing flux is large (due to the von Zeipel effect), the wind is optically thin in the Lyman continuum. This results in a high-ionization-state, fast, low-density flow. On the other hand, suppose that in the equatorial zones, which have a low surface gravity and a low flux of ionizing photons, the wind is optically thick in the Lyman continuum. Then the equatorial flow will be dense and slow with a low-ionization state—like the wind of P Cygni. Using the expected scaling laws for the effective temperature and mass-loss rates verses latitude, Lamers & Pauldrach have found that for B[e] stars, the polar flow is optically thin and the equatorial flow is optically thick in the Lyman continuum; therefore, the bi-stability mechanism may possibly explain the two-component nature of the luminous B[e] stars. However, for Be stars the mass-loss rate at the equator is too small to ever be optically thick in the Lyman continuum. They conclude, therefore, that there must be some other mechanism to further enhance or compress the equatorial outflow.

The discovery of spectral line features that can be interpreted as arising from nonradial pulsations (Vogt & Penrod 1983; Baade 1984) has led to the suggestion that nonradial pulsations may play an important role in driving an enhanced equatorial mass loss in Be stars. In a rapidly rotating star, the amplitude of the pulsation is largest for zones near the equator. Hearn (1988) has suggested that the high density of the Be star disks could perhaps arise as a consequence of the enhanced equatorial amplitude of nonradial pulsations present in rapidly rotating stars. In his picture, the pulsation gives rise to a deposition of wave energy in the subsonic portion of the flow, which increases the mass-loss rate. The line radiation pressure in the supersonic portion then produces a slow, and hence dense, equatorial outflow. The model is related to the work of Pijpers & Hearn (1989) on the production of wave-driven winds from red giant stars. Initial indications are that, for a high enough acoustic flux, the model can increase the mass-loss rate by a factor of 100 times the CAK mass-loss rate, while maintaining a terminal speed of about 150 km s^{-1} (Koninx & Hearn 1991). Unfortunately the model has the unacceptable property that the acoustic wave amplitude is greater than the speed of sound (J.-P. Koninx 1991, private communication). Details have yet to be worked out, but even if the model is not able to achieve the density concentration that is inferred for Be stars, the basic idea of accounting for the acoustic wave momentum deposition may be important.

Instead of employing a mechanism that increases the equatorial mass-loss rate, another mechanism that increases the equatorial density is the convergence of the polar flow toward the equator which results from the rapid rotation of the star. This approach requires a full two-dimensional axisymmetric model of the structure of the wind. Poe (1987) developed such a model for rotating stars, but focused primarily on the fast line-driven winds of the hotter O stars. In addition, he was only able to examine cases for which the rotation speed was less than 60% of the critical value. His results demonstrated that the streamlines converge toward the equator before turning radially outward, but the degree of convergence was small for the stars that he studied. This is because, for hotter stars, the radiation forces dominate; therefore, the radial component of the outflow is large compared to the meridional component. As a result, the density enhancement of the equatorial zone was too small and the corresponding terminal velocities were too large to explain Be stars—a conclusion which basically verified the results of the one-dimensional equatorial versus polar models. Although Poe's model does not reproduce the observations of the cooler B stars, it has, nonetheless, brought useful insight into the two-dimensional flow patterns and the degree of convergence which results from rotation.

1.3. *Synopsis*

In this paper we consider the two-dimensional flow pattern originating from the B stars and discover an additional mechanism that leads to the formation of a dense equatorial disk. In this mechanism, the disk arises as a result of the confluence of the flow from high latitudes as it converges into the equator. To study this process, we have developed an analytic approximation for the supersonic region of the flow. This supersonic approximation has the property that we may obtain the global two-dimensional axisymmetric outflow directly from the one-dimensional equatorial solution. Employing our approximate solution, we are able to explore a different region of parameter space than that explored by Poe (1987). When we match the observational constraints on the terminal velocities in the winds of Be stars, our model leads to the formation of shocks above and below the equator. These shocks compress the flow and provide a previously unknown mechanism for forming a dense equatorial disk, which may resolve the disagreement between the observed IR and UV mass-loss rates. The model predicts the observed $v \sin i$ thresholds for the onset of Be phenomena (Waters 1986; Grady et al. 1987, 1989). It also predicts the correct degree of superionization and explains the presence of C IV in the equatorial region.

The outline of this paper is as follows: In § 2 we introduce the supersonic approximation and the process for obtaining the two-dimensional solution from a one-dimensional equatorial solution of the equations of motion. In § 3 we discuss the imlications of the model for producing a dense disk, and we derive estimates of the density and thickness of the disk as well as estimates of the shock temperature. Section 4 presents the application of the model to Be stars, and we discuss the link between the dense disk and the superionization of the wind.

2. ROTATING WIND MODEL

2.1. *Fluid Equations*

A stellar wind consists of circumstellar low-density gas that has been accelerated by some external force such as radiation pressure or stellar magnetic fields. For an inviscid Newtonian fluid element of mass, m, volume, τ, density, ρ, pressure, P, and velocity, $\boldsymbol{v}$, the fluid equations that we require are the continuity equation,

$$\frac{\delta m}{\delta t} = \int_\tau \left[\frac{\partial \rho}{\partial t} + \nabla \cdot (\rho \boldsymbol{v})\right] d\tau = 0 , \tag{1}$$

and the momentum equation,

$$\frac{\delta (m\boldsymbol{v})}{\delta t} = \int_\tau \left[\frac{\partial (\rho \boldsymbol{v})}{\partial t} + \nabla \cdot (\rho \boldsymbol{v} \otimes \boldsymbol{v})\right] d\tau = \int_\tau (-\nabla P + \rho \boldsymbol{f}^{\rm ext}) d\tau , \tag{2}$$

where $\delta/\delta t$ is the Lagrangian time derivative (see, e.g., eqs. [3.1.9]–[3.1.11] in Batchelor 1967), $\otimes$ denotes the tensor product (thus $\boldsymbol{v} \otimes \boldsymbol{v}$ has components $v_i v_j$, see Schutz 1980), ∇ is the covariant derivative, and $\boldsymbol{f}^{\rm ext}$ is the total external force per unit mass on the fluid element. Note that the usual differential form of the fluid equations may be obtained by noticing that the volume element, τ, is arbitrary, which implies that the integrand of equation (1) vanishes and that the integrands of equation (2) must be equal.

In the energy equation, the radiative heating and cooling terms dominate, so the temperature of the wind is determined by the condition of radiative equilibrium. Klein & Castor (1978) have calculated the non-LTE temperature distribution in a stellar wind and find that the electron temperature is approximately constant with radius and is slightly less than the stellar effective temperature (cf. Cayrel 1963; however, see Drew 1989). Therefore, for simplicity, we make the usual assumption that the wind is isothermal with a temperature equal to the effective temperature of the star. In this case, we replace the energy equation by the isothermal equation of state,

$$P = a^2 \rho \,, \tag{3}$$

where a is the isothermal speed of sound in the wind.

We wish to model the wind from a rotating hot star. Since we are interested in the case where rotational effects dominate the flow, we cannot assume the usual spherical symmetry, but instead assume steady-state axisymmetric flow. We are interested in the luminous early-type stars, so we assume the wind is driven primarily by continuum plus line radiation forces (including the FA finite disk correction factor). With these assumptions, in spherical polar coordinates (radius, r, polar angle, θ, and azimuth, ϕ), the differential form of the continuity equation (1) becomes

$$\frac{1}{r^2}\frac{\partial}{\partial r}(r^2 \rho v_r) + \frac{1}{r \sin\theta}\frac{\partial}{\partial \theta}(\sin\theta\, \rho v_\theta) = 0 \,, \tag{4}$$

and the r-, θ-, and ϕ-components of the momentum equation (2) are, respectively,

$$\begin{aligned} v_r \frac{\partial v_r}{\partial r} + \frac{v_\theta}{r}\frac{\partial v_r}{\partial \theta} - \frac{v_\theta^2 + v_\phi^2}{r} &= -\frac{a^2}{\rho}\frac{\partial \rho}{\partial r} + f_r^{\rm ext} \,, \\ v_r \frac{\partial v_\theta}{\partial r} + \frac{v_\theta}{r}\frac{\partial v_\theta}{\partial \theta} + \frac{v_r v_\theta}{r} - \cot\theta \frac{v_\phi^2}{r} &= -\frac{a^2}{r\rho}\frac{\partial \rho}{\partial \theta} \,, \\ \frac{1}{r \sin\theta}\left(v_r \frac{\partial}{\partial r} + \frac{v_\theta}{r}\frac{\partial}{\partial \theta}\right)(r \sin\theta\, v_\phi) &= 0 \,. \end{aligned} \tag{5}$$

For a spherical star of mass, M, radius, R, luminosity, L, and electron scattering continuum opacity, σ_e, the sum of the gravitation and radiation forces is

$$f_r^{\rm ext} = -\frac{GM}{r^2} + \frac{\sigma_e L}{4\pi c r^2}\left[1 + fk\left(\frac{1}{\sigma_e \rho v_{\rm th}}\frac{dv_r}{dr}\right)^{\alpha}\right], \tag{6}$$

where f is the finite disk correction factor, given by equation (50) of CAK—see also FA. The CAK force multiplier constants, k and α, are determined by the number of optically thick lines as a function of line opacity (for appropriate values, see Abbott 1982). Abbott uses the normalization of k corresponding to selecting hydrogen for the characteristic Doppler width; therefore, $v_{\rm th} = (2kT/m_H)^{1/2}$. Note that the external forces are all central forces, which implies, with the additional assumption of axisymmetry, that the angular momentum about the rotation axis is conserved along a given streamline (see the ϕ-component of the momentum eq. [5]).

2.2. *Supersonic Approximation*

Equations (4), (5), and (6) comprise the equations for the wind of a rotating hot star that we wish to solve. Poe (1987) solved these equations numerically. However, using a numerical model, it is difficult to predict the response to changes in the various parameters. For this reason, we seek an approximation that permits us to develop an analytic solution to the model equations. For a spherically symmetric stellar wind model, such as the CAK model, gas pressure forces are unimportant in determining the fluid streamlines in the supersonic portion of the wind. A similar situation also holds in the two-dimensional momentum equation (5). As can be seen later in § 2.5, conservation of angular momentum implies that the scale of *both* v_ϕ and v_θ is set by $V_{\rm rot} R/r$. Thus we see that each of the momentum terms within equation (5) are either of $O(v_r^2)$, $O(v_r V_{\rm rot})$, or $O(V_{\rm rot}^2)$, whereas, the pressure terms are of $O(a^2)$. In early-type stars $V_{\rm rot} \gg a$; therefore, whenever v_r is also $\gg a$, the pressure terms are unimportant, *as long as the density gradient is not too large* (and r is not much greater than R). Thus, in the supersonic region, the momentum equation (2) reduces to

$$\frac{\delta(m\boldsymbol{v})}{\delta t} = \int_\tau \rho \boldsymbol{f}^{\rm ext}\, d\tau \quad (r > r_s) \,, \tag{7}$$

where the sonic point, r_s, is defined by $v_r(r_s) = a$. Equation (7) is nothing more than Newton's law of motion for free particles. In other words, when the pressure terms disappear, we effectively have a gas of noninteracting particles. Therefore, the solution to the fluid streamlines is a set of free particle trajectories determined by the external forces: gravity and radiation pressure. To determine an approximate solution for the streamline in the supersonic portion of the wind, we first need the initial conditions at the sonic point. Then, in principle, we merely need to integrate the Newtonian equations of motion for a particle to find the fluid streamline. In practice, however, we employ a one-dimensional solution of an individual streamline and adapt this solution to the particular initial conditions of each streamline.

2.3. *Flow in the Equatorial Plane*

FA have numerically solved the fluid equations (4) to (6) in the equatorial plane ($\theta = \pi/2$ and $v_\theta = 0$) of a rotating star; thus, their solution provides us with an appropriate one-dimensional solution for an individual streamline. FA give the following convenient fits to their numerical model as a function of rotation speed, $V_{\rm rot}$:

$$\begin{aligned} v_\infty &= \zeta v_{\rm esc}\left(1 - \frac{V_{\rm rot}}{V_{\rm crit}}\right)^{\gamma} \,, \\ v_r &= v_\infty\left(1 - \frac{R}{r}\right)^{\beta} \,, \\ v_\phi &= V_{\rm rot}\left(\frac{R}{r}\right) \,, \\ \dot{M} &= \frac{1}{2}\dot{M}_{\rm CAK}\left(1 - \frac{V_{\rm rot}}{V_{\rm crit}}\right)^{\xi} \,, \end{aligned} \tag{8}$$

with $\zeta \approx 2.2\alpha/(1-\alpha)$, $\beta = 0.8$, $\gamma = 0.35$, $\xi = -0.43$. We obtained the value for ξ by fitting Figure 4 of FA, and we have ignored the weak dependence on escape velocity, v_{esc}, in the equations for the terminal velocity, v_∞, and mass-loss rate, $\dot{M}$, which is really the equatorial mass flux multiplied by $4\pi R^2$. $\dot{M}_{CAK}$ is given by equation (46) of CAK, and the critical rotation speed, V_{crit}, is defined by $V_{crit} \equiv [GM(1-\Gamma)/R]^{1/2} = v_{esc}/2^{1/2}$, where $\Gamma = \sigma_e L/4\pi cGM$.

Note that in the definition of V_{crit}, FA have ignored the effects of rotation on the shape of the star [including the rotational distortion decreases the true critical speed by the factor $(2/3)^{1/2}$]. Since it is not clear how to fully correct the FA model for this effect, we must also ignore the effects of rotation on the shape of the star. At low rotation speeds, this is not a significant problem, since there is significant distortion of the star only when the star is rotating quite fast. However, one must keep in mind that when we report the ratio of a rotation speed to the critical speed, $\Omega \equiv V_{rot}/V_{crit}$, we are in general using the critical speed for a spherical star. Later we will estimate a partial correction, to these reported values of Ω, that accounts for rotational distortion.

Although the critical point of a radiatively driven flow may occur some distance from the star, the sonic location is just above the stellar surface at $r_s \approx R$. From equation (8), we obtain the following initial conditions at the sonic point in the equator:

$$\begin{aligned} r &\approx R , \\ \theta &= \pi/2 , \\ v_r &= a , \\ v_\theta &= 0 , \\ v_\phi &\approx V_{rot} . \end{aligned} \tag{9}$$

Note that the result $v_\theta = 0$ is a result of assuming that the flow is symmetric under reflections about the equatorial plane.

2.4. *Solution in the Orbital Plane*

Given that the flow in the equator is given by equation (8) with initial conditions (9), we now construct the approximate two-dimensional supersonic solution from the one-dimensional equatorial solution. Consider a fluid streamline originating at the point ($r = r_s$, $\theta = \theta_0$). The particle trajectory/streamline is determined by gravity and radiation forces, both of which are central forces. Therefore, just as in the Kepler problem, the motion of the particle will be confined to an "orbital" plane, perpendicular to the angular momentum vector, $\boldsymbol{L}$, which is conserved. The initial conditions for this streamline determine the orientation of the orbital plane, since the unit vector normal to the orbital plane may be obtained from

$$\hat{\boldsymbol{z}}' = \frac{\boldsymbol{L}}{\|\boldsymbol{L}\|} \propto \boldsymbol{r} \times \boldsymbol{v}|_{r=r_s} , \tag{10}$$

where the prime denotes the coordinate system of the orbital plane.

We next determine these initial conditions at the sonic point. The initial position is

$$r = r_s \approx R , \tag{11a}$$

$$\theta = \theta_0 . \tag{11b}$$

The r-component of the velocity is, by definition, the isothermal speed of sound,

$$v_r = a , \tag{11c}$$

and the ϕ-component of the velocity is determined by conservation of the angular momentum per unit mass about the rotation axis, that is, $L_z = RV_{rot} \sin^2 \theta(R) = rv_\phi \sin \theta(r)$. Since the sonic point occurs close to the stellar surface, we will assume that $\theta(R) \approx \theta_0$. Solving for v_ϕ at the sonic point yields

$$\begin{aligned} v_\phi &\approx V_{rot}\left(\frac{R}{r}\right)\frac{\sin^2 \theta_0}{\sin \theta(r)}\bigg|_{r=r_s} \\ &\approx V_{rot} \sin \theta_0 . \end{aligned} \tag{11d}$$

Note that this azimuthal velocity is the same as at the stellar surface.

Determining the θ-component of the velocity is more difficult. In the subsonic region of the flow, hydrostatic equilibrium dominates the forces. It is perhaps plausible (but by no means certain) that the subsonic flow will be primarily along the gradient of the pressure. Ignoring the rotational distortion of the isopressure surfaces, this direction will be primarily radial. Based on these arguments we will *assume* that $v_\theta \ll v_\phi$ at $r = r_s$, in which case the effective boundary condition on the θ-component is

$$v_\theta \approx 0 . \tag{11e}$$

From equation (10), we see that, as long as $v_\theta \ll v_\phi$, the unit vector perpendicular to the orbital plane is

$$\hat{\boldsymbol{z}}' \approx \hat{\boldsymbol{r}}_0 \times \hat{\boldsymbol{\phi}}_0 . \tag{12}$$

This implies that the orbital plane is inclined by the angle

$$i = \frac{\pi}{2} - \theta_0 , \tag{13}$$

with the line of nodes along the y-axis (see Fig. 1).

Using this orientation of the orbital plane (eqs. [12] and [13]) we transform the initial conditions at the sonic point (11) to the orbital plane coordinate system, which gives

$$\begin{aligned} r' &\approx R , \\ \theta' &= \pi/2 , \\ v'_r &= a , \\ v'_\theta &\approx 0 , \\ v'_\phi &\approx V_{rot} \sin \theta_0 . \end{aligned} \tag{14}$$

These initial conditions for an arbitrary latitude, equation (14), are identical to the equatorial initial conditions, equation (9), except for the modification of v_ϕ. Note, however, that this modification to v_ϕ is equivalent to choosing a different stellar rotation rate.

We now know the initial conditions to employ at an arbitrary latitude when we determine the location of the streamlines. Next, we must determine how to adapt the equatorial solution (8) to find the solution of the inclined orbit. Note that given equivalent initial conditions and forces, the particle trajectory in the inclined orbit will be identical to the trajectory in the equator. We have already seen that, as long as we choose the appropriate rotation rate, the initial conditions are the same. The external forces consist of gravity and a density-dependent radiation pressure. If we assume that the stellar

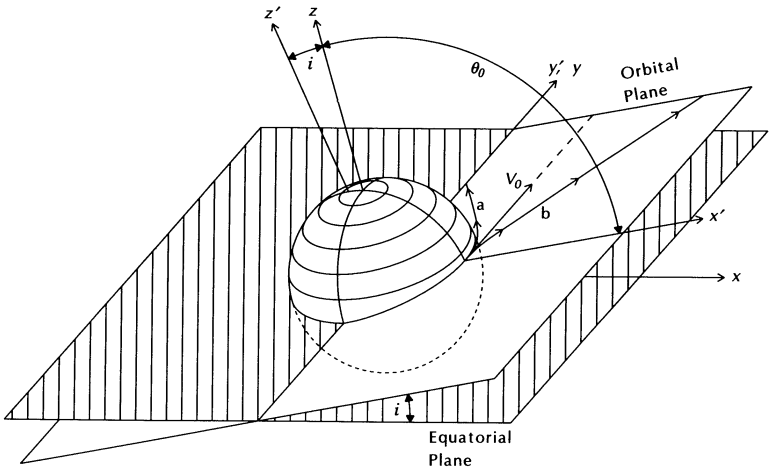

FIG. 1.—Orientation of the "orbital" plane for streamlines originating at polar angle θ_0. The orbital plane is inclined by an angle i about the y-axis. The dashed line shows the direction of the initial velocity vector, v_0. The streamline labeled (a) denotes a case where the rotation speed of the wind is high, and the streamline labeled (b) denotes a case with a low rotation speed. Note that in case (a) the streamline crosses the equator at an azimuth $\phi' = \pi/2$.

surface is nearly spherical and that the density diverges with distance approximately like the equatorial solution, then the forces due to radiation and gravity will be the same in both the inclined orbit and in the equator. Therefore, subject to the approximations above, the inclined trajectory will be the same as the equatorial trajectory. Thus, we may obtain the solution in the inclined orbit directly from the equatorial solution (8) by merely replacing $V_{\rm rot} \rightarrow \sin\theta_0\, V_{\rm rot}$, which yields

$$
\begin{aligned}
v_\infty(\theta_0) &= \zeta v_{\rm esc}\left(1 - \sin\theta_0 \frac{V_{\rm rot}}{V_{\rm crit}}\right)^{\gamma}, \\
v'_r(r,\theta_0) &= v_\infty(\theta_0)\left(1 - \frac{R}{r}\right)^{\beta}, \\
v'_\phi(r,\theta_0) &= \sin\theta_0\, V_{\rm rot}\left(\frac{R}{r}\right), \\
\dot{M}(\theta_0) &= \frac{1}{2}\dot{M}_{\rm CAK}\left(1 - \sin\theta_0 \frac{V_{\rm rot}}{V_{\rm crit}}\right)^{\xi},
\end{aligned}
\tag{15}
$$

where $\dot{M}(\theta_0)$ is the mass flux multiplied by $4\pi R^2$.

To find the trajectory in the inclined orbit, we can obtain a differential equation for the trajectory by dividing v'_r by v'_ϕ which gives

$$
\frac{dr}{d\phi'} = \frac{r^2}{R}\left[\frac{v_\infty(\theta_0)}{\sin\theta_0\, V_{\rm rot}}\right]\left(1 - \frac{R}{r}\right)^{\beta}. \tag{16}
$$

This has the solution

$$
\phi' = \frac{1}{1-\beta}\left[\frac{\sin\theta_0\, V_{\rm rot}}{v_\infty(\theta_0)}\right]\left(1 - \frac{R}{r}\right)^{1-\beta}. \tag{17}
$$

Note that as $r \rightarrow \infty$, the particle trajectory becomes radial with an asymptotic value for ϕ' of

$$
\phi'_{\rm max} = \frac{1}{1-\beta}\left[\frac{\sin\theta_0\, V_{\rm rot}}{v_\infty(\theta_0)}\right]. \tag{18}
$$

An important consequence of this asymptotic behavior is the possible existence of two classes of trajectories (shown in Fig. 1), which are distinguished by large versus small $\phi'_{\rm max}$. Case (a) trajectories cross the equator and have a large value for $\phi'_{\rm max}$, while case (b) trajectories are mostly radial and have a small value for $\phi'_{\rm max}$. We can see from equation (18) that there are four possible ways to obtain large versus small values of $\phi'_{\rm max}$:

1. Different rotation speeds, $V_{\rm rot}$. For small $V_{\rm rot}$, the trajectory (labeled b) initially curves outward and up from the straight line trajectory (dashed line) and has a small value for $\phi'_{\rm max}$. For large $V_{\rm rot}$, the trajectory (labeled a) curves inward and down from the straight line, and has a large value for $\phi'_{\rm max}$.
2. Different values of the initial latitude, θ_0. Trajectories originating near the pole, where $\sin\theta_0$ is low, will be mostly radial (trajectory b); whereas, trajectories originating at low latitudes, where $\sin\theta_0$ is large, may deflect down toward the equator (trajectory a).
3. Different values of v_∞. Large terminal speeds correspond to trajectory (b), and low terminal speeds correspond to trajectory (a).
4. Different values of the velocity law exponent, β. Slow velocity laws (large β) correspond to case (a) trajectories, and fast velocity laws (small β) correspond to case (b) trajectories.

The physical cause of the behavior associated with equation (18) will be discussed later in § 3.1.

2.5. *Transformation to Stellar Coordinates*

Given the location of the streamline in the orbital plane, equation (17), we can transform back to stellar coordinates. From the spherical triangle in Figure 2*a*, we obtain the following coordinate transformation:

$$
\begin{aligned}
\cos\theta &= \cos\theta_0 \cos\phi', \\
\sin\phi &= \frac{\sin\phi'}{\sin\theta}, \\
\cos\phi &= \frac{\tan\theta_0}{\tan\theta},
\end{aligned}
\tag{19}
$$

and from Figure 2*b*, for the velocity transformation we obtain

$$
\begin{aligned}
v_r &= v'_r, \\
v_\phi &= v'_\phi \cos\psi = \frac{V_{\rm rot} R}{r}\frac{\sin^2\theta_0}{\sin\theta}, \\
v_\theta &= v'_\phi \sin\psi = \frac{V_{\rm rot} R}{r}\frac{\sin\theta_0 \cos\theta_0}{\sin\theta}\sin\phi'.
\end{aligned}
\tag{20}
$$

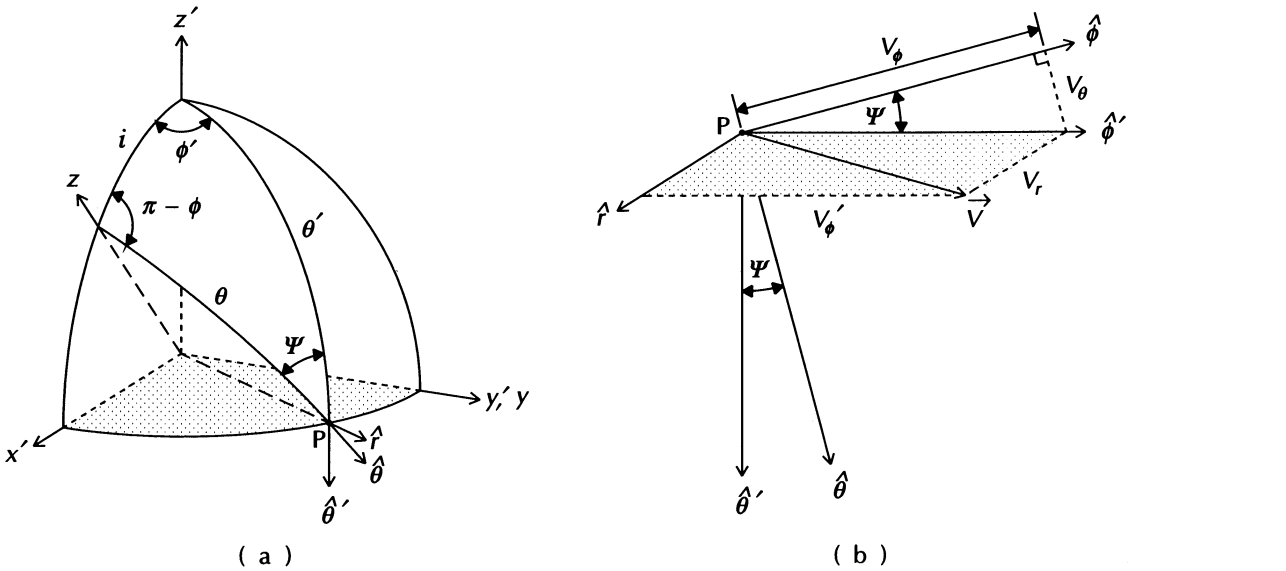

FIG. 2.—(*a*) Spherical triangle used for obtaining the coordinate transformation from the orbital plane (primed) coordinates to stellar (unprimed) coordinates at the point *P*. The dotted region indicates the orbital plane. (*b*) Velocity transformation from orbital to stellar coordinates. Note that the orbital plane (dotted region) is perpendicular to the page.

Note that the scale of *both* v_ϕ and v_θ is set by $V_{\rm rot}\,R/r$. This is a consequence of the conservation of the total angular momentum, and is brought about by a combination of Coriolis and centrifugal forces.

2.6. *Wind Density*

Using our knowledge of the fluid streamlines, we can obtain the density in the wind from the continuity equation. Consider the stream tube shown in Figure 3. Mass conservation requires that

$$\frac{\dot{M}(\theta_0)}{4\pi}\sin\theta_0\,d\theta_0\,d\phi_0 = \rho v_r r^2 \sin\theta\,d\theta\,d\phi\,. \tag{21}$$

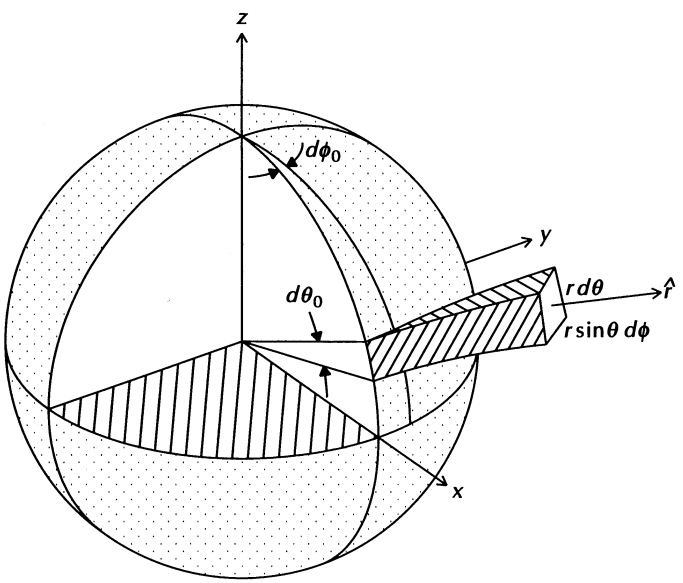

FIG. 3.—Stream tube used for obtaining the density in the wind. Note that rotational invariance implies that $d\phi = d\phi_0$; however, $d\theta$ is not constant in general.

Rotational symmetry implies that the streamlines are invariant under a rotation by $d\phi_0$ about the *z*-axis; therefore, $d\phi = d\phi_0$. Solving for ρ then gives

$$\rho = \frac{\dot{M}(\theta_0)}{4\pi r^2 v_r (d\mu/d\mu_0)}\,, \tag{22}$$

where $\mu = \cos\theta$. We may evaluate $d\mu/d\mu_0$ by starting with equation (19), from which we get

$$\frac{d\mu}{d\mu_0} = \cos\phi' - \mu_0 \sin\phi' \frac{d\phi'}{d\mu_0}\,,$$

$$= \cos\phi' + \frac{\cos^2\theta_0}{\sin\theta_0}\frac{d\phi'}{d(\sin\theta_0)}\sin\phi'\,. \tag{23}$$

From equation (17) we find

$$\frac{d\phi'}{d(\sin\theta_0)} = \frac{\phi'}{\sin\theta_0}\left[1 - \sin\theta_0 \frac{d\ln v_\infty}{d(\sin\theta_0)}\right], \tag{24}$$

and from equation (15) we obtain

$$\frac{d\ln v_\infty}{d(\sin\theta_0)} = \frac{-\gamma V_{\rm rot}/V_{\rm crit}}{1 - \sin\theta_0\, V_{\rm rot}/V_{\rm crit}}\,. \tag{25}$$

Inserting equations (25) and (24) into equation (23) we finally find

$$\frac{d\mu}{d\mu_0} = \cos\phi' + \cot^2\theta_0\left(1 + \gamma\frac{\sin\theta_0\, V_{\rm rot}/V_{\rm crit}}{1 - \sin\theta_0\, V_{\rm rot}/V_{\rm crit}}\right)\phi'\sin\phi'\,. \tag{26}$$

This equation in conjunction with equation (22) provides the wind density.

2.7. *Model Summary*

Our model for the approximate two-dimensional supersonic flow from a rotating star consists of equations (15), (17), (19), (20), (22), and (26) which provide the position, velocity, and

density of a streamline originating at θ_0 parameterized as a function of radius. One may thus construct the entire two-dimensional supersonic approximate solution by mapping the streamlines $[\theta(r), \phi(r)]$ for successive values of the starting polar angle θ_0 (although an individual streamline does not lie at constant azimuth ϕ, employing rotational symmetry eliminates the ϕ-dependence of the global solution). Alternatively, given a location (r, θ), one must iteratively solve equations (17) and (19) to first find θ_0 of the streamline passing through that location prior to evaluating the velocities and density.

3. MODEL RESULTS

We wish to investigate the geometry of the supersonic streamlines predicted by our model and the implications for the winds from rotating hot stars. The behavior of the streamlines is quite sensitive to the ratio $\zeta \equiv v_\infty/v_{esc}$. If this ratio is large, the flow velocity increases rapidly and the effects of rotation are small. On the other hand, if ζ is small (near unity), then the flow velocity increases slowly and the effects of rotation can be quite pronounced. Unfortunately, theoretical values of v_∞ (and hence ζ) do not agree with the observational values for B stars. Reasonable values for the CAK parameter α are about 0.5 for B stars (Abbott 1982); this implies a theoretical value of $\zeta \approx 2.2$ (see eq. [8]). Figure 4 shows the observed values of ζ for main-sequence stars. These values of ζ range from about 3.5 for early O stars to less than one for late B stars. Thus, for B stars, the value of ζ is significantly below the theoretical value. Given the interesting dynamical effects associated with the observed values of ζ, we have decided to treat ζ as a free parameter in our model.

In the following three subsections, we first discuss the geometry of the streamlines in the wind, which leads to the formation of an equatorial disk under certain circumstances. Then we estimate the physical properties of this disk, and finally we discuss the connection between the formation of the disk and the presence of superionized elements.

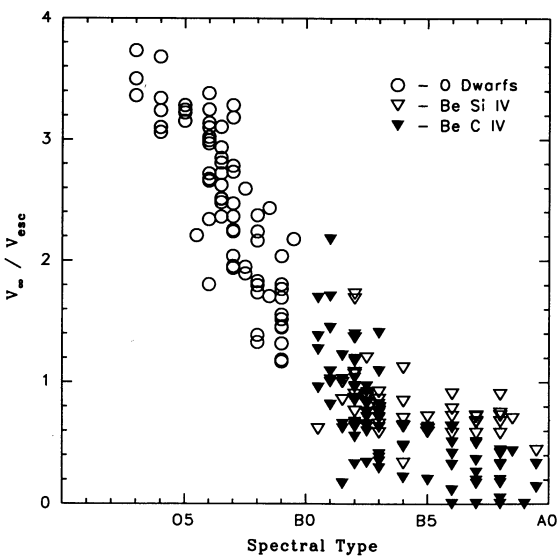

FIG. 4.—Observed values of the ratio of terminal wind speed to stellar escape speed, $\zeta \equiv v_\infty/v_{esc}$, vs. spectral type. Note the rapid increase in going to stars earlier than B2 which means that these earlier-type stars are less likely to have an equatorial disk. (For O stars we used the estimates of the terminal speed from Prinja, Barlow, & Howarth 1990, and for the Be stars we used the edge-velocities from K. S. Bjorkman 1989. The escape speeds are from Table 1.)

3.1. *Wind Properties*

To map the entire two-dimensional flow we first selected a grid of initial polar angles, θ_0, for the streamlines. We then stepped through a radial grid from 1 to 10 stellar radii to map each of the streamlines. As we stepped through the radial grid we evaluated the position, velocity, and density of the fluid at that point.

Figure 5 shows the streamlines originating at 5° intervals on the stellar surface for selected values of $\Omega \equiv V_{rot}/V_{crit}$ with $\zeta \equiv v_\infty/v_{esc} = 1$. To suppress the azimuthal motion we plotted only the z and ϖ coordinates of the streamlines, where z is the height above the equator and ϖ is the distance from the rotation axis. Rotational symmetry thus implies that the flow originating at θ_0 lies in the surface of revolution (about the z-axis) generated by the associated curve in Figure 5. Therefore, these surfaces of revolution are the "flow sheets" from the star. Note that for large V_{rot} the streamlines originating near the equator eventually cross the equator; whereas, those streamlines originating near the pole never cross the equator. These are the two characteristic solutions alluded to earlier in reference to Figure 1. Furthermore, note that for low rotation rates, only the noncrossing streamlines exist; however, above some threshold rotation rate, both equator-crossing and noncrossing streamlines exist.

Let us now explore the physical origin of the equator-crossing streamlines. To deflect the fluid towards the equator, there must be a zone near the star where there is a physical force (in the nonrotating reference frame) which has a downward component towards the equator (in the $-\hat{z}$ direction). The only physical forces acting in the supersonic approximation of our model are gravity and radiation pressure, both of which are radially directed. Therefore, the only way a net force with a negative z-component can result is if gravity exceeds the radiation force, which implies that the equator-crossing streamlines can only arise when this situation occurs.

We can see this behavior illustrated in Figure 1 where we changed the rotation rate. For small V_{rot}, the noncrossing trajectory, case (b), initially curves outward and up from the straight line trajectory. This positive curvature indicates that the net physical force points outward, which in turn implies that the radiation forces must initially exceed gravity. For large V_{rot}, the equator-crossing trajectory, case (a), initially curves inward and down from a straight line. This negative curvature indicates that the net physical force initially points inward, which implies that the radiation forces are initially smaller than gravity. Note that there can still be an outward motion because of centrifugal forces.

In our model, we do not directly deal with the forces, but instead we are using mathematical curve fits to the FA model. Therefore the mechanism whereby gravity can exceed the radiation force (in the supersonic region) is obscured. To discover the mathematical origin of this behavior in our model, recall that $v_r(r) \propto v_\infty$, which implies that the sum of the forces in the rotating frame, $f_{rad} + f_{grav} + f_{cent}$, $\propto dv_r/dt \propto v_r\, dv_r/dr \propto v_\infty^2$. By arbitrarily changing ζ, and hence v_∞, or by changing the centrifugal force, f_{cent}, we implicitly change the radiation force in such as way as to maintain this scaling relationship. One concern with arbitrarily reducing ζ to match the terminal speed of B stars is the validity of this implicit mathematical scaling of the radiation forces in relation to the gravitational

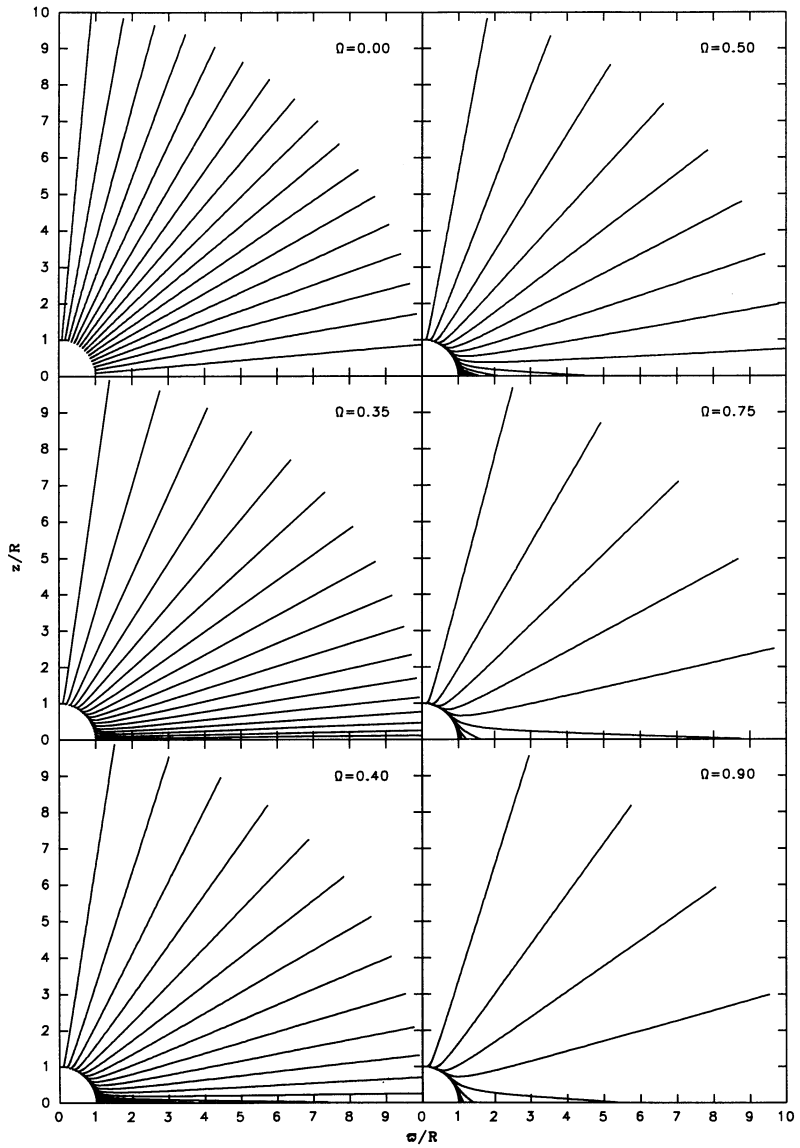

FIG. 5.—Streamlines for various values of the rotation rate $\Omega \equiv V_{\rm rot}/V_{\rm crit}$ for a B2 star where $\zeta = 1$. The streamlines originate at 5° increments in latitude, thus the separation between streamlines is an indication of the density in the wind. Note that the ϕ-component of the motion is not shown in this figure, thus the flow sheet from a given latitude is the surface of revolution of the appropriate curve in this diagram. Note also that for $\Omega > 0.4$ the streamlines cross the equator, and for larger Ω, the streamlines from a larger fraction of the star cross the equator.

force. Since we are not actually solving the full set of fluid equations using a set of CAK parameters which give a low value of ζ, we cannot be certain that the radiation force actually scales in this fashion.

To determine that the implicit scaling relationship is plausible and to verify that, in fact, gravity can exceed the radiation force in the supersonic region of a rotating wind, we modified the FA model to include the dependence of the CAK force multiplier, $M(t)$, on n_e/W (Abbott 1982). Including this dependence accounts for changes in the ionization balance which affect the force multiplier and results in a lower terminal speed of the wind (see Kudritzki et al. 1989). This allows us to obtain a reasonably low terminal speed with realistic CAK parameters (we will present the results of this modification in a future paper). With this modification, the force multiplier (the second term inside the brackets in eq. [6]) is given by

$$M(t) = fk\left(\frac{n_e/W}{10^{11}\ \mathrm{cm}^{-3}}\right)^{\delta} t^{-\alpha}, \qquad (27)$$

where f is the finite disk correction factor, n_e is the electron number density, $W = 0.5\{1 - [1 - (R/r)^2]^{1/2}\}$ is the dilution factor, and $t = \sigma_e \rho v_{\rm th}(dv_r/dr)^{-1}$ is the optical depth parameter. The FA model is reproduced by choosing $\delta = 0$ (cf. eq. [6]). For a B star with $T_{\rm eff} = 20{,}000$ K we get (after fitting a power law to k over the range of n_e/W) from Table 2 of Abbott (1982) that $k = 0.6$, $\alpha = 0.5$, and $\delta = 0.17$.

Using these CAK parameters and the modified force multiplier (27), we solved the r-component of the momentum equation (5) in the equatorial plane. For a zero rotation rate case,

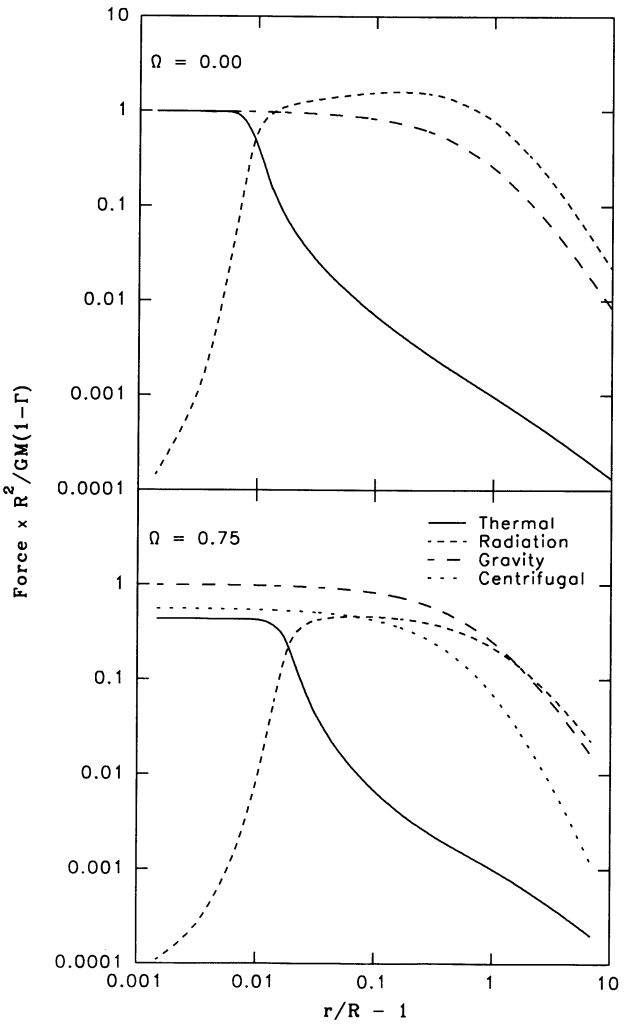

FIG. 6.—Forces vs. radius in an equatorial one-dimensional rotating wind model that has $v_\infty/v_{esc} = 1.4$. Note that in the nonrotating case, $\Omega = 0$, the radiation force exceeds gravity once the pressure support is lost, which occurs near the sonic point. In the rapidly rotating case, $\Omega = 0.75$, the radiation force does not exceed gravity until the centrifugal support is lost.

the large value of δ reduces the terminal speed ratio to $\zeta = 1.4$, which is relatively close to the observed value of $\zeta = 1$. The mass-loss rate is $\dot{M} = 3.6 \times 10^{-10}\, M_\odot\ \mathrm{yr}^{-1}$, which agrees with mass-loss rates derived by Snow (1981). The corresponding forces are shown in Figure 6 as a function of radius for the nonrotating case as well as rapidly rotating case. Note in the nonrotating case that the radiation force exceeds gravity at a radius of $1.01R$, which is the sonic point in the wind (as evidenced by the rapid drop in the gas pressure); however in the rotating case, gravity exceeds the radiation force out to a radius of about $3R$, which is well beyond the sonic point. Thus gravity can in fact exceed the radiation force in the supersonic region and produce a net component of the force towards the equator. To maintain a smoothly accelerating flow in the nonrotating case, the radiation force must support the flow once the gas pressure disappears; this is why the radiation force exceeds gravity in the supersonic portion of the flow. In the rotating case, however, the centrifugal force can support the flow to much larger radii than can the gas pressure (which effectively disappears at the sonic point), and it is only after the centrifugal support is lost that the radiation force must support the flow. Therefore if the star is rotating rapidly enough that the centrifugal force provides a major component of the support, then gravity will exceed the radiation force in the region between the sonic point and the point where the centrifugal support is lost. If this region is sufficiently large, then, in the nonrotating reference frame, the fluid will experience a net force toward the equator for a long enough duration that the streamline will cross the equator.

The centrifugal support is largest at the equator and decreases with increasing latitude. For this reason, if the rotation rate is large enough that there are equator-crossing streamlines, the equator-crossing streamlines will originate in a zone of latitudes centered about the equator. Of the equator-crossing streamlines, the streamline which crosses the equator closest to the star is the streamline that originates at $\theta_0 = \pi/2 - \epsilon$, where ϵ is infinitesimal. An important aspect of the equator-crossing solutions is that the radius at which the first streamline crosses the equator is not the stellar surface, but rather a finite distance away from the star. We call this initial crossing radius the convergent point, since most of the streamlines cross the equator just beyond this location. To determine this location, note that when a streamline intersects the equator, $\phi' = \pi/2$ (see Fig. 1). Solving the trajectory equation (17) for r at $\phi' = \pi/2$ for the streamline originating at $\theta_0 = \pi/2 - \epsilon$ gives, in the limit $\epsilon \to 0$,

$$\frac{r_{con}}{R} = \left\{1 - \left[\frac{\pi\zeta(1-\beta)(1 - V_{rot}/V_{crit})^{\gamma}}{\sqrt{2}\, V_{rot}/V_{crit}}\right]^{1/(1-\beta)}\right\}^{-1} . \quad (28)$$

Figure 7 shows the convergent point location verses rotation rate, Ω, for several values of the terminal speed ratio, ζ. Note that for a specific value of ζ, the location of the convergent point starts at infinite radius and moves inward as the rotation rate is increased above the threshold rotation rate. Conversely, for a specific value of Ω, changing the value of ζ changes the disk location.

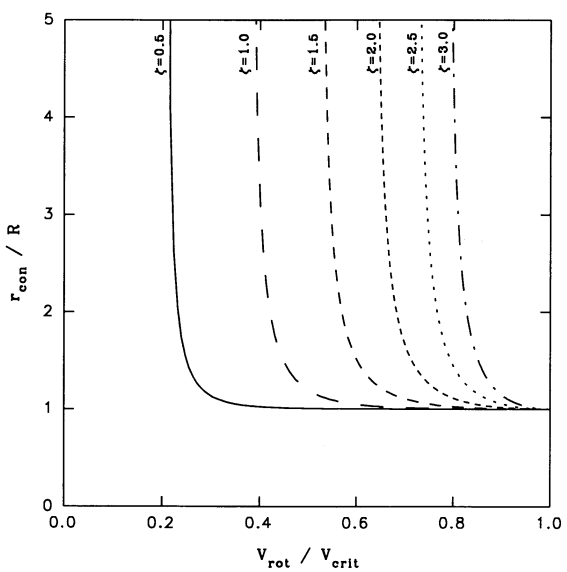

FIG. 7.—Convergent point location vs. rotation rate for several values of the terminal speed ratio $\zeta \equiv v_\infty/v_{esc}$. For each ζ, note that as the rotation rate is increased above the threshold rotation rate, the convergent point moves inward. This implies that the detached disk forms closer to the star at higher rotation rates.

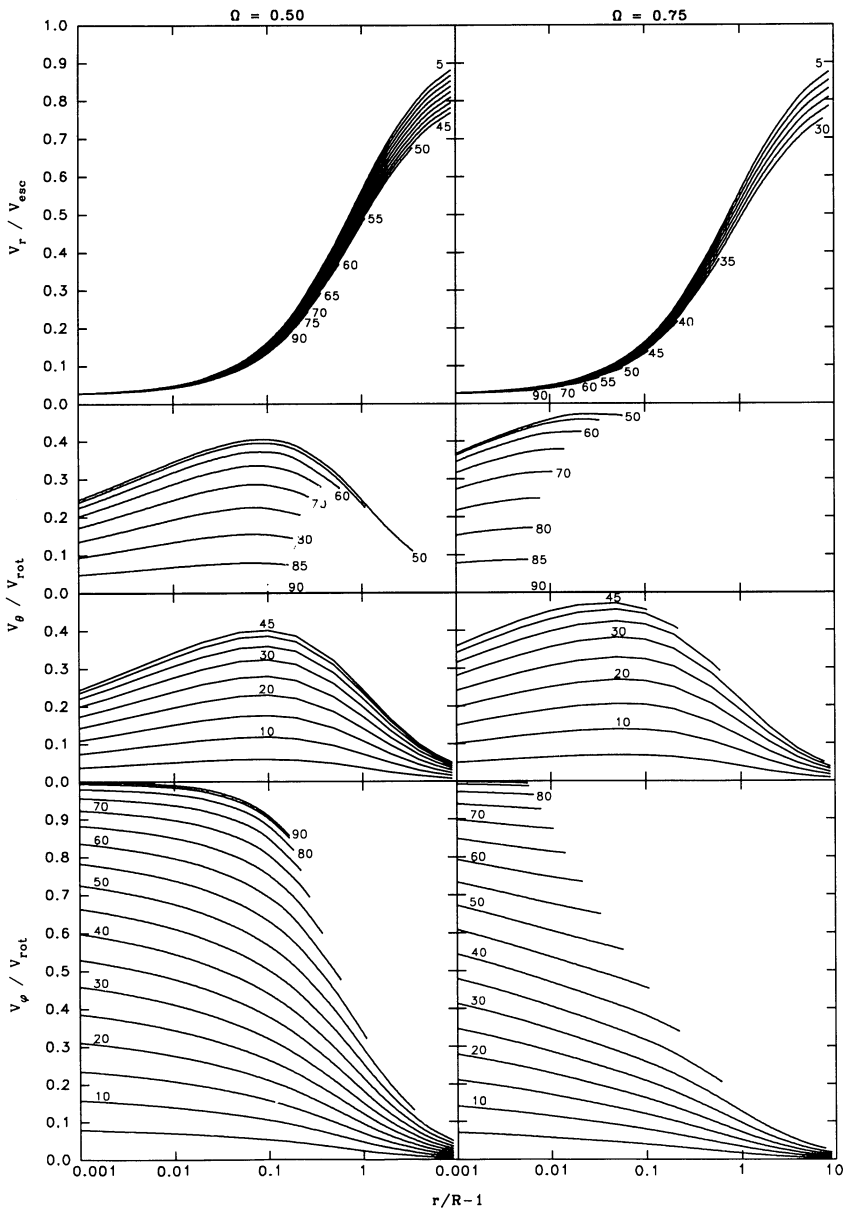

FIG. 8.—Velocity components of individual streamlines for two values of the rotation rate, Ω, with $\zeta = 1$. The curves are labeled according to their initial polar angle θ_0. The curves terminate when the streamline crosses the equator ($\theta = \pi/2$). Note that the termination point marked 90 on the abscissa corresponds to the convergent point.

Figure 8 shows the r-, θ-, and ϕ-components of the velocity for two typical rotation rates for which there are equator-crossing streamlines. The velocities are plotted as a function of radius with each curve corresponding to a given streamline, labeled according to its initial polar angle, θ_0. The curves terminate when the streamline crosses the equator, so the velocity of the fluid entering the equator may be determined from the locus of termination points. Note that, for $\Omega = 0.75$, the flow entering the equator has a maximum value of $v_\theta/V_{rot} \approx \frac{1}{2}$, which occurs at $r \approx 1.1R$.

Figure 9 shows the density in the wind for the same cases as Figure 8. Again, the locus of termination points provides the density of the wind as it enters the equator. Note that near the equator, the wind density can be a factor of 10 larger than at the pole. Also note that, in the pole, the density is lower than the equivalent zero rotation rate model. We know that the equatorial flow must remain in the equator (by symmetry); therefore, as the streamlines cross the equator, the specific volume of the fluid goes to zero, implying that the density diverges (note that we have terminated the streamlines at the equator, so this divergence is not seen on the plot in Fig. 9, except in the region near the convergent point). The large density implies that the pressure terms will dominate the momentum equation, and our approximate solution breaks down in the equatorial region at the convergent point and beyond.

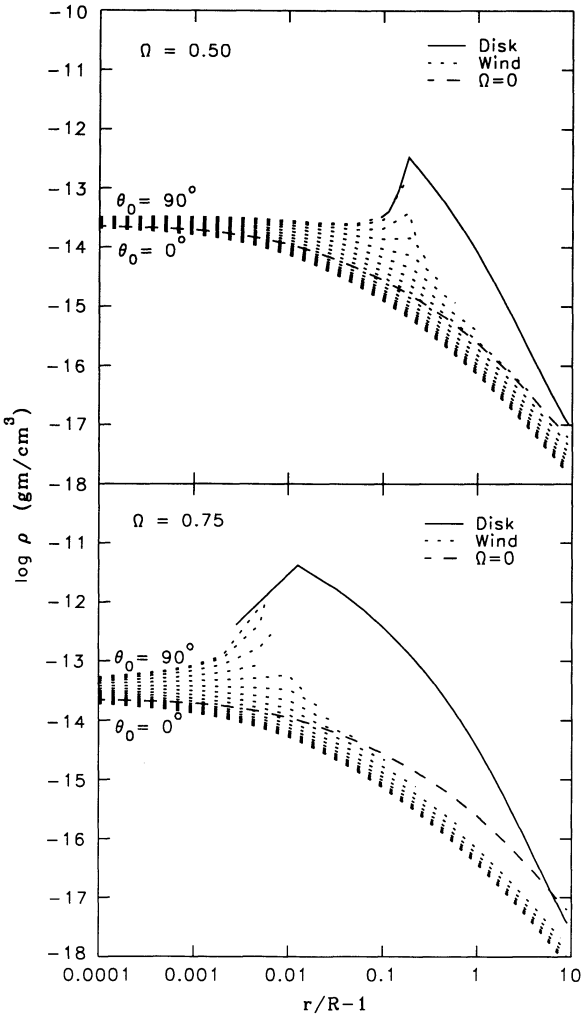

FIG. 9.—Density along individual streamlines (*short dashed lines*) for two values of the rotation rate, Ω, with $\zeta = 1$. Again the curves terminate when the streamline crosses the equator. The density of a zero rotation rate model is shown for comparison (*medium dashed line*). Note that using zero rotation rate model for the polar flow is not very accurate. The solid line gives the density of the disk (from Fig. 17).

3.2. *Disk Formation*

We now investigate the consequences of the situation in which the streamlines cross the equator and our approximations break down. Streamlines cannot cross each other since the large density creates a pressure which will ultimately turn the flow. Above some threshold value of the rotation rate, the component of the flow velocity perpendicular to the equator, $v_z = -v_\theta|_{\theta=\pi/2}$, is supersonic for some streamlines and subsonic for others as they enter the equatorial region; whereas, the r-component is supersonic everywhere. If the θ-component is subsonic, then an ordinary pressure gradient will suffice to turn the flow parallel to the equator. However, if both the r- and θ-components are supersonic, then the information that the flow must be parallel to the equator will no longer to be able to propagate upstream. In this case, a standing oblique shock must develop to turn these streamlines. To determine the radial location of these shocks, we must therefore determine which streamlines have a supersonic θ-component of the velocity as they cross the equator. Note that although the initial location of the shock is determined by the θ-component, it is the slope of the shock that determines the actual mixture of the r- and θ-components that are reduced across the shock.

From the locus of termination points in Figure 8, we see that the θ-component of the fluid velocity can only be supersonic beyond the convergent point, which implies that $r_{sh}^{min} > r_{con}$, where r_{sh}^{min} is the minimum shock radius. Hence, it is only somewhere beyond the convergent point that the standing shock first forms, and it is thus detached from the star. Furthermore the wind originates in both the northern and southern hemispheres of the star; thus, the equatorial flow will be bounded by standing shocks above and below the equator (see Fig. 10). We call the compressed flow in the region between the shocks the "equatorial disk," and the flow in the region outside the shock the "stellar wind."

To form the disk, the rotation rate must be large enough that some streamlines "cross" the equator. The condition for some streamlines to cross the equator is $\phi'_{max} > \pi/2$ for at least some range of θ_0. Solving equation (18) for the required rotation rate for the streamline originating at θ_0 gives the crossing condition

$$\frac{V_{rot}}{V_{crit}} > \frac{\pi}{\sqrt{2}} \frac{\zeta(1-\beta)}{\sin\theta_0} \left(1 - \sin\theta_0 \frac{V_{rot}}{V_{crit}}\right)^{\gamma} . \quad (29)$$

Since $\sin\theta_0 < 1$, a lower limit to the threshold velocity required for crossing the equator may be obtained by choosing $\theta_0 = \pi/2$, giving the equator-crossing threshold,

$$\left(\frac{V_{rot}}{V_{crit}}\right)_{th} = \frac{\pi}{\sqrt{2}} \zeta(1-\beta)\left(1 - \frac{V_{rot}}{V_{crit}}\right)^{\gamma} . \quad (30)$$

Equation (29) implies that, for any rotation rate above this threshold, some of the wind will attempt to cross the equator and thereby be added to the disk. Note, however, that the threshold for forming the standing shock and dense disk will be somewhat higher than that given by equation (30), since, as we noted earlier, the shock will form only if the velocity component perpendicular to the equator is supersonic for at least some of the equator-crossing streamlines. Figure 11 shows the threshold rotation rate as a function of terminal speed ratio, ζ, using the equator-crossing threshold (eq. [30]—filled circles) and using the supersonic requirement (filled diamonds). Note that the supersonic condition only requires a threshold rotation rate, Ω_{th}, about 0.04 larger than the crossing threshold. Therefore, equation (30) is a fairly good approximation to the disk formation threshold.

So far, we have been ignoring the effects of rotational distortion; however, we can estimate the correction to the rotation threshold that arises from rotational distortion. First, we note that the mass flux and terminal speed for any streamline are mostly determined by local conditions at the stellar surface, so for each streamline we replace the distorted star by a spherical star with identical mass and luminosity, but whose radius matches the photospheric radius of that streamline. Now the rotation threshold is determined from the equatorial streamlines, and the equatorial radius as a function of rotation rate is given by

$$R_{eq}(\Omega_d) = \frac{R}{1 - (1/3)\Omega_d^2} , \quad (31)$$

where Ω_d is the ratio of the rotation speed of the true, that is, distorted star, critical speed. Note that $R_{eq} = (3/2)R$ at the

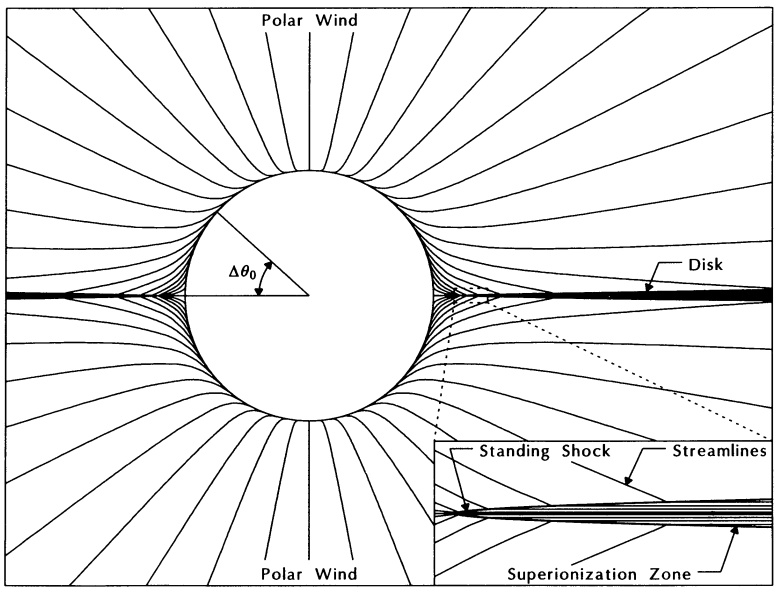

FIG. 10.—Diagram of the dense disk produced by the standing shock in the wind, where $\zeta = 1$ and $\Omega = 0.5$. The shock turns the flow parallel to the equator (see inset), thereby preventing the streamlines from crossing at the equator. Note that the disk is detached from the star, and the shock temperature is responsible for the superionization zone.

critical speed, $\Omega_d = 1$. Dividing Ω_d by the spherical star threshold rotation ratio, Ω_{th}, gives

$$\frac{\Omega_d}{\Omega_{th}} = \frac{(V_{rot}/V_{crit})_d}{(V_{rot}/V_{crit})_{th}} = \sqrt{\frac{(3/2)R}{R_{eq}(\Omega_d)}}, \tag{32}$$

and solving for Ω_d we obtain the distorted star correction to the disk formation threshold

$$\Omega_d = \sqrt{\frac{(3/2)\Omega_{th}^2}{1 + (1/2)\Omega_{th}^2}}. \tag{33}$$

Note that since this expression ignores gravity darkening and its effect on the radiative flux and terminal speed, it must only be considered a partial correction to the rotation threshold.

If the star is rotating faster than the disk formation threshold, only some fraction of the total mass loss will be added to the disk. The material which is added to the disk (see Fig. 10) is the wind that arises from the equatorial zone on the star which has polar angles in the range

$$\frac{\pi}{2} - \Delta\theta_0 < \theta_0 < \frac{\pi}{2} + \Delta\theta_0 . \tag{34}$$

We find, from the crossing condition equation (29), that

$$\cos\Delta\theta_0 = \frac{\pi}{\sqrt{2}} \frac{\zeta(1-\beta)}{V_{rot}/V_{crit}} \left(1 - \cos\Delta\theta_0 \frac{V_{rot}}{V_{crit}}\right)^{\gamma} . \tag{35}$$

Thus, the fraction of the stellar surface whose streamlines form the disk is the solid angle of this zone (given by eq. [34]) divided by 4π. This yields $\sin\Delta\theta_0$. This fraction is shown in Figure 12 as a function of rotation rate for several different values of the terminal speed ratio. Note that for rotation rates slightly above the disk formation threshold that approximately half of the stellar wind goes into the disk.

The total mass-loss rates into the equatorial disk and the polar wind can be obtained by integrating the mass-loss rate in equation (15) over the two appropriate zones on the stellar surface. This gives

$$\dot{M}_d = \frac{1}{2}\dot{M}_{CAK}\int_0^{\mu_d}\left(1 - \sqrt{1-\mu^2}\frac{V_{rot}}{V_{crit}}\right)^{\xi} d\mu ,$$

$$\dot{M}_w = \frac{1}{2}\dot{M}_{CAK}\int_{\mu_d}^{1}\left(1 - \sqrt{1-\mu^2}\frac{V_{rot}}{V_{crit}}\right)^{\xi} d\mu , \tag{36}$$

where $\mu_d = \cos(\pi/2 - \Delta\theta_0) = \sin\Delta\theta_0$. Hereafter a sub(super)-script d denotes the disk, and a sub(super)script w denotes the polar wind. In deriving this equation we have assumed that the mass-loss rate from the star is unaffected by the presence of the disk. This is justified since the flow entering the disk is super-

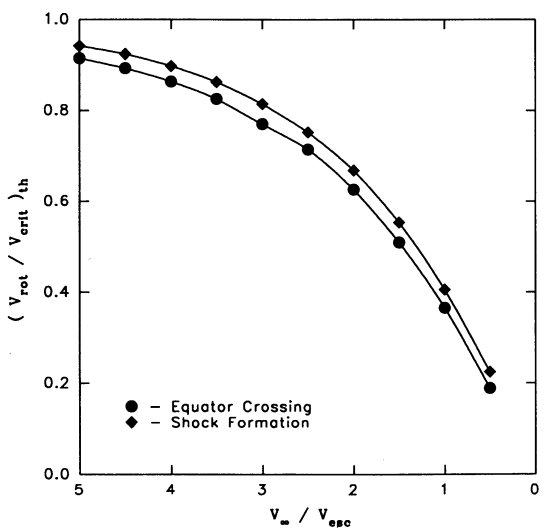

FIG. 11.—Disk formation threshold vs. the ratio of terminal speed to escape speed. Note that the supersonic threshold (shock formation) is only slightly higher than the equator crossing threshold. Also note that for higher terminal speed ratios, the star must rotate more rapidly to form a disk.

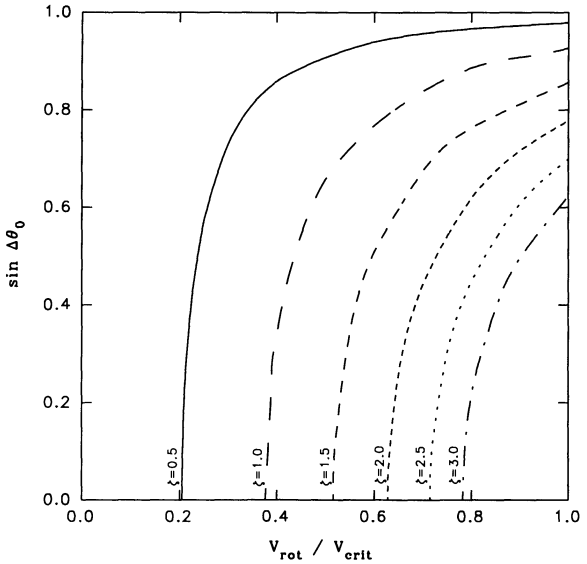

FIG. 12.—Fraction of the stellar surface, sin $\Delta\theta_0$, whose streamlines enter the disk vs. rotation rate (shown for several values of ζ). Note that, for $\zeta = 1$, a rotation rate $\Omega = 0.42$ (barely above the disk formation threshold) is large enough that half of the stellar mass loss enters the disk.

sonic and information about the disk cannot travel back upstream from the shock.

3.3. *Disk Properties*

We next discuss some of the dynamics of the disk so that we can make order of magnitude estimates of the disk properties. The disk turns out to be quite thin, so we describe the disk with a one-dimensional model where we assume that the disk variables are only a function of ϖ. The purpose of the shock/pressure gradient in the equator is to turn the flow that enters the disk parallel to the equator, so we will assume $v_z^d = 0$. Although we will not present a complete solution of the model of the disk dynamics in this paper, we can make some useful estimates of the disk properties from the equations of such a model. Consider the differential volume element in Figure 13.

Balancing each component of the forces acting on the volume element with the momentum fluxes entering/leaving the element leads to the following three conclusions:

1. *z-component.* The pressure in the disk, P_d, must balance the z-component of momentum flux entering the disk; thus

$$P_d = \left\{P_w + \rho_w\left[v_z^2 - v_z v_\varpi\left(\frac{dz_{sh}}{d\varpi}\right)\right]\right\}\Bigg|_{z=z_{sh}}, \qquad (37)$$

where z_{sh} is the height of the shock above the equatorial plane and the slope of the shock, $dz_{sh}/d\varpi$, is related to the shock angle, α_{sh}, by $dz_{sh}/d\varpi = \tan\alpha_{sh}$ The wind pressure, P_w, density, ρ_w, and velocity components, v_z and v_ϖ, are evaluated immediately prior to the shock.

2. ϕ-component. The ϕ-component of the disk velocity is governed by conservation of angular momentum in the disk after accounting for the angular momentum deposited by the wind. One interesting consequence is that the rotation velocity of the disk will initially decrease faster than $1/r$ (the usual assumption based on angular momentum conservation in the equator). This is because material with lower specific angular momentum is added to the disk from the wind. Eventually, at large radii, material is no longer added to the disk, so the rotation speed asymptotically approaches a $1/r$ falloff. Note that this behavior may have observational consequences in the shape of the Hα emission-line wings.

3. ϖ-*component.* The equatorial radial momentum equation (7) of FA must be extensively modified. First, there is additional radial momentum deposited by the wind. Second, the density dependent radiation forces must be modified, since the density is determined by equation (37) instead of falling as $1/r^2$ as FA assumed. Last, since the ϕ-component of the disk velocity is different from that assumed by FA, the centrifugal forces arising from the ϕ-component of the motion change as well.

These three conclusions imply that the disk dynamics are substantially different from the usual one-dimensional equatorial models. Therefore, to determine the velocity structure of the disk will require a new numerical model which includes the modifications listed above.

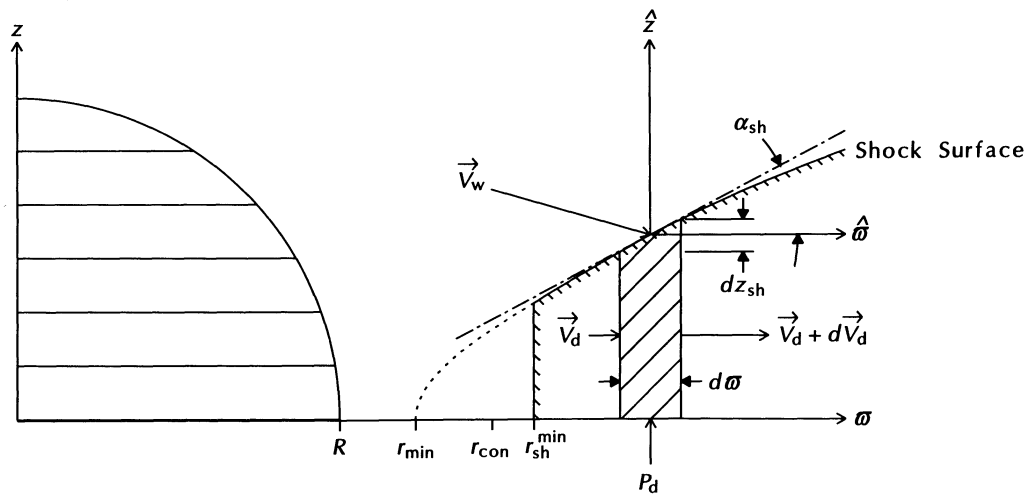

FIG. 13.—Differential volume element (*hatched region*) used for obtaining fluid equations for the disk. Also shown are the ad hoc curve used for the disk surface in the preshock region (*dashed line*) and the shock location (*hatched line*). Note that the leading edge of the shock occurs within the disk at a location beyond the convergent point.

To estimate the postshock density, we assume that the shocked material quickly cools until it is in radiative equilibrium and that the disk equilibrium temperature is also the same as the wind equilibrium temperature, that is, we employ the isothermal wind approximation. Substituting the isothermal equation of state (3) into equation (37) gives

$$\frac{\rho_d}{\rho_w} = \left\{1 + \left[\left(\frac{v_z}{a}\right)^2 - \left(\frac{v_z}{a}\right)\left(\frac{v_\varpi}{a}\right)\left(\frac{dz_{\rm sh}}{d\varpi}\right)\right]\right\}\Bigg|_{z=z_{\rm sh}} . \quad (38)$$

The disk density, equation (38), is determined from conservation of momentum in the disk. Next, we consider mass conservation. One usually uses the continuity equation to determine the density in the fluid; however, in this case, the disk density is already fixed by the z-component of the momentum equation. Instead, the differential form of the continuity equation determines the slope of the shock. This implies that the thickness of the disk is determined by the total mass-loss rate in the disk, that is, the shocks adjust their separation to accommodate the accumulated flow in the disk, $\dot{M}_d(\varpi)$. The accumulated flow in the disk consists not only of the original equatorial mass loss from the star, but also additional mass added to the disk from the wind interior to the current location, ϖ. This may be obtained by first finding the initial polar angle of the streamline entering the disk at this point, $\theta_0(\varpi, z_{\rm sh})$, and then integrating the mass-loss rate of equation (15) from this polar angle up to the equator, which gives

$$\dot{M}_d(\varpi) = \frac{1}{4}\dot{M}_{\rm CAK}\int_0^{\mu_0}\left(1 - \sqrt{1-\mu^2}\,\frac{V_{\rm rot}}{V_{\rm crit}}\right)^{\xi} d\mu , \quad (39)$$

where $\mu_0 = \cos\theta_0(\varpi, z_{\rm sh})$. Note that this is the flow in the upper half of the disk; the total flow is twice this value.

The integral form of the continuity equation for the disk is

$$\dot{M}_d(\varpi) = 2\pi\varpi^2 \tan\Delta\theta\, \rho_d v_\varpi^d , \quad (40)$$

where $\dot{M}_d(\varpi)$ is given by equation (39), and $\Delta\theta$ is the half-width (half opening angle) of the disk, that is, $\tan\Delta\theta = z_{\rm sh}/\varpi$. Note that $\Delta\theta$ is a function of radius, so the disk does not have a constant opening angle. Unfortunately, to find $\Delta\theta$, one must first solve the radial momentum equation to obtain v_ϖ^d, which we cannot obtain within the context of our present model. Instead, we will make an estimate for the slope of the disk surface (note that this will cause various inconsistencies in the description of the disk—usually in one of v_ϖ^d, $z_{\rm sh}$, or $dz_{\rm sh}/d\varpi$). Assuming that the slope of the disk surface is continuous, we see that when the disk first forms in the equator, its surface must initially be perpendicular to the radial direction. The disk is quite thin, so for simplicity we let the disk surface be parameterized by a hyperbola with the appropriate opening angle. For the minimum radius of the hyperbola, we have used the midpoint between the convergent point and the stellar surface. This is to account for the density gradient which turns the flow in the region inside the convergent point, that is, *before* the shock forms. What we are really doing here is balancing the z-component of the momentum flux entering this hyperbola (disk) with the pressure at the equator. This hyperbola is merely a mathematically convenient surface to use in the integral form of the fluid equations and is not necessarily a shock. Specifically we have chosen

$$z_{\rm sh} = \tan(\Delta\theta)\sqrt{\varpi^2 - r_{\rm min}^2} , \quad (41)$$

where $r_{\rm min} = (R + r_{\rm con})/2$.

The shock first forms within the disk at $\varpi = r_{\rm sh}^{\rm min}$. The shock starts in the equator as a strong (subsonic downstream) shock normal to the flow in the disk since the flow already in the disk does not need to be turned. The shock then turns as it merges with the disk surface and becomes a strong oblique shock which is responsible for turning the flow entering the disk. Eventually it becomes a weak (supersonic downstream) oblique shock since, far away from the star, the flow only needs to be deflected by a small angle.

Figure 13 illustrates our assumed geometry for the shock. The dashed line, starting at $r_{\rm min}$, is the hyperbolic surface of the disk in the region prior to the shock. The shock (solid line with cross hatching) starts at $r_{\rm sh}^{\rm min}$ and merges with the hyperbola to become the disk surface. Note that the discontinuity in the shock slope as it merges with the disk surface is an artifact of our assumptions.

We still need an estimate of the disk opening angle, $\Delta\theta$, to use in the ad hoc shock surface equation (41), so consider the following order of magnitude argument. The polar wind mass loss is given by

$$\dot{M}_w(r) = 2\pi r^2(1 - \sin\Delta\theta)\langle\rho_w\rangle v_r , \quad (42)$$

where $r^2 = \varpi^2 + z_{\rm sh}^2$, and $\langle\rho_w\rangle$ is the solid angle averaged density in the polar wind. We see in Figure 5 that the separation between streamlines is approximately constant at latitudes outside the equatorial region. This implies that the average density in the wind is approximately the same as the density at the pole, that is, $\langle\rho_w\rangle \approx \rho_{\rm pole}$. Using this approximation, dividing equation (40) by (42) and solving for $\Delta\theta$ under the assumption that the disk is thin gives

$$\Delta\theta \approx \left(\frac{\dot{M}_d}{\dot{M}_w}\right)\left(\frac{\rho_{\rm pole}}{\rho_{\rm d}}\right)\left(\frac{v_r}{v_\varpi^d}\right) . \quad (43)$$

To make a rough approximation, note from Figure 8 that for rotation rates somewhat above the threshold for disk formation, $\sin\Delta\theta_0 \approx 0.5$, which implies $\dot{M}_d \approx \dot{M}_w$. Hence, equation (43) reduces to

$$\Delta\theta \approx \left(\frac{\rho_{\rm pole}}{\rho_d}\right)\left(\frac{v_r}{v_\varpi^d}\right) . \quad (44)$$

Since this equation depends on the velocity in the disk, we will have to rely on observations to make this estimate of the disk opening angle. Once we have this estimate, we will then use our ad hoc curve for the disk surface to estimate the slope of the shock.

3.4. *Postshock Zone and Superionization*

We have obtained estimates of the density and thickness of the disk, and next we turn our attention to the interface between the disk and wind. Initially, the wind is heated by the shock. The shock temperature is (Krolik & Raymond 1985)

$$T_{\rm sh} = 1.4 \times 10^5\ {\rm K}\left(\frac{v_{\rm sh}}{100\ {\rm km\ s^{-1}}}\right)^2 , \quad (45)$$

where $v_{\rm sh}$ is the component of the fluid velocity perpendicular to the shock, so the shock temperature also depends on the slope of the shock. The temperature is typically on the order of a few 10^5 K. At these temperatures, the shocked material cools primarily via EUV continuum recombination and O IV line radiation at a wavelength $\approx$200 Å (see Fig. 3*c* of Kato 1976). If we assume that the entire excess internal energy of the shocked

material is released radiatively in the EUV, then (since we know the mass-loss rate through the shock) we can estimate the EUV luminosity from

$$L_{\rm EUV} \approx \dot{M}_d C_V (T_{\rm sh} - T_d) , \quad (46)$$

where C_V is the specific heat per unit mass in the wind. The large shock temperatures will collisionally produce local superionization as the wind enters the disk and cools. Since the parallel velocity component is unchanged by the shock, the velocity of the thermally ionized species will be near the terminal velocity; furthermore, they will be strongly concentrated toward the equator. Note that our geometry for the disk superionization zone (see Fig. 10) is qualitatively similar to the scenario proposed by Marlborough, Snow, & Slettebak (1987), although our superionization mechanism is entirely different. The shock temperature depends on the stellar rotation rate; therefore, if the superionization is in fact produced thermally by the shock, we predict that the observed maximum stage of ionization will correlate with the stellar rotation rate. Note however, that we cannot calculate the shock temperature for the initial portion of the shock that occurs within the disk. Since the inner disk radius moves inward with increasing rotation rate (see Fig. 7), it is reasonable to assume that the velocity of this portion of the shock will decrease with increasing rotation rate. If it turns out that this portion of the shock dominates the production of the superionization, then the highest stage of superionization will be anticorrelated with the rotation rate.

If the shock temperature is large enough (i.e., when the rotation rate is near critical), then the resultant X-ray flux may be large enough to be observed with *ROSAT*; also the spectrum may be hard enough to produce superionization via the Auger effect (Cassinelli & Olson 1979). Since the mean free path of the X-rays is large in the polar regions, superionization will occur not only at the edge of the disk, but also in the polar regions. Therefore, in this scenario, there will be a much less pronounced equatorial concentration of the species than in the pure thermal case.

The disk is not the only mechanism for producing shocks and superionization in the wind. As is well known, radiatively driven winds are unstable (e.g., Owocki & Rybicki 1984) and this instability leads to the formation of reverse shocks which travel outward from the star (Owocki, Castor, & Rybicki 1988). These shocks are generally believed to be the source of the superionization in the rapid O star winds, and it is possible that shocks also exist in the slower winds of early B stars (MacFarlane & Cassinelli 1989). However, the shock strength must scale with the terminal velocity of the wind; therefore, we expect that the wind instability shocks will decrease in relative importance for the later spectral types. Note also that the instability produces these shocks regardless of whether or not the star is rotating. This implies that these shocks will be present to the same degree in both rotating and nonrotating stars and, therefore, cannot be used to explain the excess level of superionization present in Be stars versus normal B stars (Grady et al. 1987). Grady et al. indicate that the excess C IV equivalent width may be attributed entirely to the presence of blueshifted discrete absorption components (DACs). Furthermore, it is the presence of these DACs and not C IV itself that indicates a rotation threshold of $v \sin i > 200$ km s^{-1}. This suggests that the underlying C IV profile is produced by the wind instability shocks, while the DACs are produced by the disk.

In addition to superionization, the increased density of the disk (after it cools subsequent to the shock) will significantly enhance the IR free-free emission as well as the Hα emission produced by the star. An interestng facet of the Hα profiles observed in Be stars is that they exhibit double-peaked emission profiles rather than P Cygni profiles. This indicates that the expansion velocity of the flow in the disk is low (on the order of 10 km s^{-1} or less). Since our model indicates that the initial shock is perpendicular to the equator, the shock is initially a strong shock, and as a result the postshock velocity is initially subsonic. This is near the location where the disk compression is a maximum, so we expect the disk expansion velocity to be subsonic in the region that contains the highest disk densities; therefore this subsonic region should dominate the Hα formation. Beyond the region of maximum compression, the density rapidly falls as the ram pressure of the wind decreases and the expansion velocity of the disk increases. Although our model does not address the details of the radial expansion in the disk, it does qualitatively appear that the model will predict double-peaked Hα emission profiles.

4. APPLICATION TO Be STARS

As an application of our model, we turn to the class of hot stars which seems to exhibit the largest effects of rotation upon the stellar wind, namely Be stars. Our model appears to naturally account for many of the discrepancies in the observations of these stars and may provide a basis for a unified interpretation of the results in many different spectral regions. For the remainder of the discussion, we will choose parameters for a typical B2 star: $M = 8.3\ M_\odot$, $R = 4.5\ R_\odot$, $T = 23{,}000$ K (Popper 1980; Hayes 1978). This gives a critical rotation rate $V_{\rm crit} = 590$ km s^{-1}.

4.1. *Threshold Rotation Speed*

In the context of our model, we interpret the Be phenomena as being associated with the formation of the disk in the wind of a rotating star. To form the disk, we saw in equation (30) that there is a threshold rotation rate which depends on the terminal velocity of the wind. Observationally, one measures the edge velocity of UV resonance lines. Assuming that the edge velocity is representative of the terminal velocity of the wind, we have for B2e stars that the ratio of terminal velocity to escape velocity is $\zeta \approx 1$; whereas, for O6 stars $\zeta \approx 2.7$ (see Fig. 4). The threshold rotation rate from equation (30) is

$$\frac{V_{\rm rot}}{V_{\rm crit}} \approx \begin{cases} 0.75 & \text{O6 stars} \\ 0.37 & \text{B2 stars} \end{cases} , \quad (47)$$

and when we require that v_z be supersonic at the equator we get (see Fig. [11])

$$\frac{V_{\rm rot}}{V_{\rm crit}} \approx \begin{cases} 0.79 & \text{O6 stars} \\ 0.41 & \text{B2 stars} \end{cases} . \quad (48)$$

Estimating the correction for the rotational distortion from equation (33), we find

$$\frac{V_{\rm rot}}{V_{\rm crit}} \approx \begin{cases} 0.84 & \text{O6 stars} \\ 0.48 & \text{B2 stars} \end{cases} . \quad (49)$$

Using the true critical rotation rate $V_{\rm crit} = 480$ km s^{-1} gives a Be star rotation threshold of $V_{\rm rot} > 230$ km s^{-1}. For a uniform distribution of inclination angles, $\langle \sin i \rangle = \pi/4$ so the observed threshold should occur at $\langle v \sin i \rangle > 180$ km s^{-1}. This is

TABLE 1

DISK FORMATION THRESHOLD OBTAINED FROM THE OBSERVED VALUE OF THE TERMINAL SPEED FOR VARIOUS MAIN-SEQUENCE SPECTRAL TYPES

Spectral Type	$T_{\rm eff}$ [a] (K)	R [b] ($R_\odot$)	M [c] ($M_\odot$)	$v_{\rm esc}$ (km s^{-1})	$V_{\rm crit}$ [d] (km s^{-1})	$v_\infty/v_{\rm esc}$ [e]	$\Omega_{\rm th}$ [f]	$(V_{\rm rot})_{\rm th}$ [f] (km s^{-1})
O3	49000	14	55	850	600 (490)	3.6	0.87 (0.91)	520 (450)
O6.5	40000	10	29	940	660 (540)	2.7	0.78 (0.84)	520 (450)
B0	32000	6.6	15	910	640 (520)	1.4	0.53 (0.61)	340 (320)
B2	23000	4.5	8.3	840	590 (480)	1.0	0.41 (0.48)	240 (230)
B5	15000	3.3	4.5	720	510 (420)	0.8	0.33 (0.39)	170 (160)
B9	10000	2.6	2.6	620	440 (360)	0.75	0.31 (0.37)	140 (130)

[a] Values are smoothed values from Hayes 1978.

[b] The values for O stars are from Howarth & Prinja 1989 and for B stars they are smoothed values from Popper 1980.

[c] The masses for O stars are obtained from the effective gravity given by Kudritzki & Hummer 1990. See also Kudritzki et al. 1992. For B stars they are smoothed values from Popper 1980.

[d] The numbers in parentheses are the true critical rotation speed (i.e., accounting for the rotational distortion of the star).

[e] Values for v_∞ are spectral type averages, and for O stars are obtained from Prinja et al. 1990. For B stars they are edge-velocities from K. S. Bjorkman 1989.

[f] The numbers in parentheses are calculated using the rotational distortion correction eq. (33). These numbers are presented to give an estimate of the uncertainty due to rotational distortion.

lower, but it agrees approximately with the threshold value of $v \sin i$ for the onset of IR excesses in Be stars (Waters 1986). A similar (but somewhat lower) threshold has been observed for the presence of discrete C IV absorption components as well as for the presence of narrow absorption cores in Si II (Grady et al. 1987, 1989). Other models for Be stars that increase the equatorial mass-loss rate to achieve the high densities required for the disk (e.g., Poe & Friend 1986) generally require unrealistically high rotation rates.

In going from B2 toward earlier spectral types, we see from Figure 4 that there is a rapid rise in terminal velocity of the wind. From Figure 11 we see in turn that this implies that earlier spectral types must rotate faster to form a disk. Using the observed values of the terminal speed, we calculated the rotation threshold as a function of main-sequence spectral type, and the results are summarized in Table 1. Presumably, the higher the rotation threshold, the less likely a star will rotate fast enough to form a disk. Thus the dependence of the terminal speed on spectral type naturally explains why the frequency of Be stars is large at B2 and decreases toward earlier spectral types (which also explains why there are very few Oe stars). However, in our model, the decrease in frequency of Be stars later than B2 must be explained in a different way. This is because the terminal velocity inferred from observations slowly decreases later than B2, which implies that the frequency of Be stars should slowly rise instead of falling as observed. However, this discrepancy may be explainable in the following way.

One problem with using the measured edge velocity for the terminal speed in B stars is that the line profiles become quite weak, especially for the later spectral types. Thus determining the edge velocity (where the line profile returns to the continuum) becomes quite difficult and may in fact be systematically underestimated. For this reason we have also investigated the theoretical behavior of the terminal speed verses spectral type. As we mentioned earlier in § 3.1, to obtain realistic values for the terminal speed of the wind, we must include the dependence of the force multiplier on the ionization balance in the wind by including the parameter δ. Non-LTE calculations of k, α, and δ have been made for O stars (Pauldrach et al. 1990); however, these calculations have not been performed for main-sequence B stars. For that reason we must use the values determined by Abbott (1982), which assume optically thin geometrically diluted ionizing radiation. Although these assumptions break down for the massive O star winds (see Pauldrach 1987 for a detailed discussion), Abbott's calculations should be more reliable for the much weaker B star winds. Table 2 lists our adopted values for k, α, and δ. Note that for the B stars, we interpolated the values of k and α versus n_e/W from Table 2 of Abbott (1982). We then obtained δ by fitting a power law to k over the range of n_e/W for each spectral type. The mass-loss rate, terminal wind speed, and n_e/W were determined using the "cooking recipe" of Kudritzki et al. (1989). Figure 14 shows the comparison of the observed and theoretical values of the terminal speed. Note that for early spectral types the agreement is reasonably good, but at late spectral types there is large disagreement. An inter-

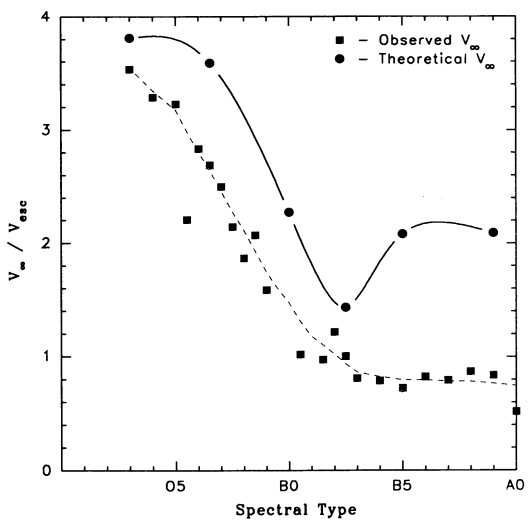

FIG. 14.—Ratio of terminal speed of the wind to stellar escape speed vs. spectral type. The solid curve is obtained from the theoretical values of the terminal speed, listed in Table 2, and the dashed curve is obtained using the terminal speeds from the observations shown in Fig. 4. Note that the theoretical terminal speed ratio has a minimum at spectral type B2.

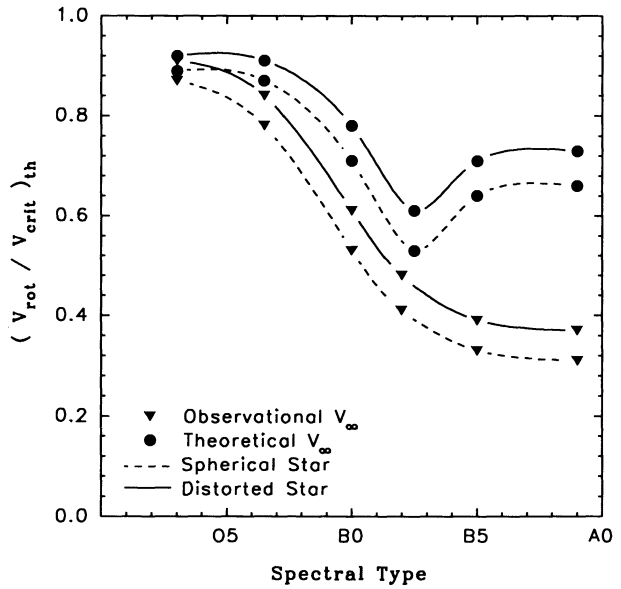

FIG. 15.—Ratio of the rotation speed to critical speed required for disk formation verses spectral type. The dashed lines are obtained assuming no rotational distortion of the star, and the solid lines are obtained using eq. (33) to estimate the rotational distortion correction. Note that when using the theoretical values of the terminal speed, the threshold has a minimum value near B2, the spectral type at which Be stars are most prevalent.

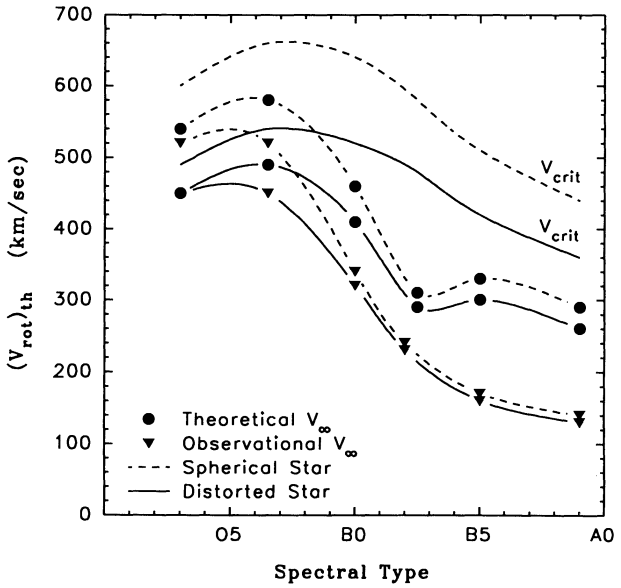

FIG. 16.—Disk formation threshold rotation speed vs. spectral type. Curves are shown with and without the rotational distortion correction. The thresholds are calculated using either the observational or theoretical estimates of the terminal speeds. Also shown for reference is the critical rotation speed.

esting feature of the theoretical curve is the minimum exhibited at B2. This implies that the disk formation threshold would also have a minimum at B2. Figure 15 shows the disk formation thresholds using both the observed and theoretical values of the terminal speed verses spectral type, and the corresponding rotation speeds are shown in Figure 16 (the numerical results are summarized in Table 2). We see from these figures that if we accept the theoretical values of the terminal speed verses spectral type, then our model predicts that the maximum frequency of Be stars should occur near B2 and (depending on spectral type) the threshold rotation velocity is around 300 km s^{-1}.

4.2. *Disk Density*

To find the disk density verses radius, we must first make an estimate of the disk opening angle, $\Delta\theta$, to use in the disk surface equation (41). At a rotation rate of 75% of the critical speed, the maximum shock compression occurs at about $1.1R$ where v_z has its maximum value of $0.5V_{\rm rot}$ (see Fig. 8). If we assume the slope of the shock is small (since the shock turns out to be quite thin), then we get, from the disk density equation (38), a compression ratio of

$$\frac{\rho_d}{\rho_w} \approx \left(\frac{v_z}{a}\right)^2 \approx \frac{1}{4}\left(\frac{V_{\rm rot}}{a}\right)^2 \approx 200 . \qquad (50)$$

From Figure 9, we see that the wind density at the equator, ρ_w (i.e., just before it passes through the shock), is about a factor of 4 higher than the density at the pole. Thus the density compression from pole to disk is

$$\frac{\rho_d}{\rho_{\rm pole}} \approx 800 . \qquad (51)$$

In addition to the density ratio, we also need to know the velocity ratio, for which we rely on observations. Observations of Hα as well as of Be X-ray binaries (Waters et al. 1988) indicate that the terminal velocity in the disk is $v_\varpi^d \approx 150$ km s^{-1}. UV spectral lines indicate that $v_r \approx 1000$ km s^{-1} (Snow

TABLE 2

DISK FORMATION THRESHOLD OBTAINED FROM THE THEORETICAL VALUES OF THE TERMINAL SPEED FOR VARIOUS MAIN-SEQUENCE SPECTRAL TYPES

$T_{\rm eff}$ (K)	Spectral Type[a]	k[b]	α[b]	δ[b]	n_e/W ($\rm cm^{-3}$)	$\dot{M}$[c] ($M_\odot$ $\rm yr^{-1}$)	$v_\infty/v_{\rm esc}$[c]	$\Omega_{\rm th}$[d]	$(V_{\rm rot})_{\rm th}$[d] (km s^{-1})
50000.....	O3	0.017	0.74	0.115	10^{13}	9.1×10^{-6}	3.81	0.89 (0.92)	540 (450)
40000.....	O6.5	0.060	0.68	0.067	10^{12}	3.1×10^{-7}	3.59	0.87 (0.91)	580 (490)
30000.....	B0	0.159	0.60	0.118	10^{11}	2.7×10^{-8}	2.27	0.71 (0.78)	460 (410)
20000.....	B2.5	0.609	0.51	0.166	$10^{9.5}$	3.6×10^{-10}	1.43	0.53 (0.61)	310 (290)
15000.....	B5	0.220	0.51	0.018	10^{8}	9.8×10^{-12}	2.08	0.64 (0.71)	330 (300)
10000.....	B9	0.427	0.52	0.038	$10^{7.5}$	1.3×10^{-12}	2.09	0.66 (0.73)	290 (260)

[a] Approximate spectral type for the temperature given.
[b] Values for O3 stars are from Kudritzki et al. 1992. For O6.5 stars they are from Pauldrach et al. 1990, and for B stars they are from fits to the CAK parameters verses n_e/W given in Table 2 of Abbott 1982.
[c] Mass-loss rates and terminal speeds (with no rotation) are obtained using the "cooking recipe" of Kudritzki et al. 1989.
[d] The numbers in parentheses are calculated using the rotational distortion correction eq. (33). These numbers are presented to give an estimate of the uncertainty due to rotational distortion.

1981). Using these observational results for the velocity ratio, equation (44) gives a disk opening angle of

$$\Delta\theta \approx 10^{-2} \approx 0.^{\circ}5 . \quad (52)$$

Combining IR excesses with optical polarization data, Bjorkman & Cassinelli (1990) have shown that there are two thicknesses of disks which are consistent with the data: either a thick disk $\Delta\theta \approx 50°$, or a thin disk $\Delta\theta < 15°$, (typically a few $0.^{\circ}1$). Our model is consistent with the disk alternative.

Using our estimated disk opening angle in the disk surface equation (41) we can make an estimate of the shock slope. Employing this slope in the disk density equation (38), a more refined estimate of the disk density is shown in Figure 17 for three values of the rotation rate. From measurements of the IR excess, Waters et al. (1987) estimate typical base densities of the disk to be $\rho_0 \approx 10^{-12}$ to 10^{-11} g cm^{-3}, which is in good agreement with our maximum disk densities. This is an indication that perhaps our model provides enough compression; however, the measured densities are model dependent. For example, in the IR excess model, Waters et al. assumed that $\Delta\theta$ had a constant value of 15°. For a constant opening angle, the measured base density scales as $\rho_0 \propto 1/(\Delta\theta)^{1/2}$. Our model predicts an opening angle 30 times smaller than that assumed by Waters et al.; however, our disk does not have a constant opening angle, and the radial dependence of the density is quite different as well; therefore, we must really perform the calculations of the IR excess and UV line equivalent widths predicted by our model to know for certain whether our model can explain the discrepancy between the UV and IR mass-loss rates.

We should also mention that any mechanism which increases the equatorial mass-loss rate (e.g., acoustic waves or the bi-stability mechanism) may be invoked in addition to our model to raise the disk density even further.

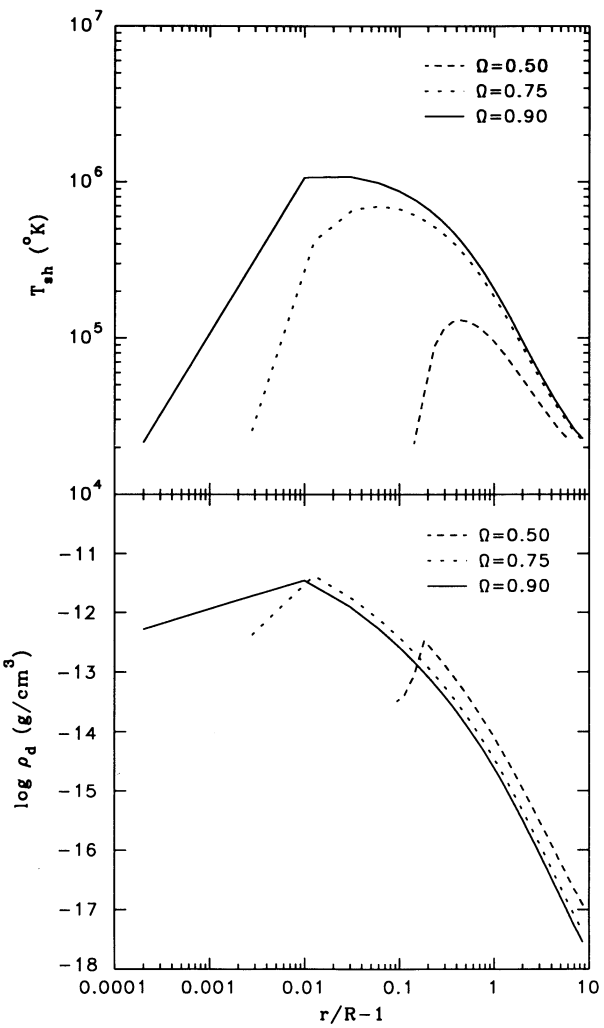

FIG. 17.—Shock temperature and disk density as a function of radius for three values of the rotation rate, Ω. The maximum temperatures are sufficient to produce superionization and EUV radiation. Note the increase in the maximum shock temperature as the rotation rate increases. At the highest rotation rates, the temperature is large enough to produce soft X-rays.

4.3. *Shock Structure*

We next examine the structure of the standing shocks adjacent to the disk and its implications for UV spectral lines. To obtain the shock temperature, we must know the velocity of the wind perpendicular to the shock, which again requires an estimate of the slope of the shock. Our previous estimate, equation (41), consisted of an ad hoc curve whose minimum radius was inside the convergent point; however, the shock forms outside the convergent point. To account for this, we have used our ad hoc curve, but only calculated the shock temperature at those locations where the velocity component perpendicular to the shock is supersonic. This does not, however, account for the portion of the shock that occurs within the disk which, in any case, cannot be calculated since we do not know the disk velocity. The results of the shock temperature calculation are shown in Figure 17. With a rotation velocity of 300 km s^{-1}, the shock temperature is

$$T_{sh} \approx 10^5 \text{ K} \quad (53)$$

at the radius where the shock compression is a maximum. Combining this shock temperature with a typical UV mass-loss rate of $\dot{M} = 10^{-10} M_{\odot}$ yr^{-1} (Snow 1981), we find an EUV luminosity from equation (46) of

$$L_{EUV} \approx 10^{29} \text{ ergs s}^{-1} \approx 10^{-7.8} L_{bol} . \quad (54)$$

Because of the low temperature, this is far below the detection threshold of the *Einstein* satellite, but may have been detected by *ROSAT* for high rotation rate, low hydrogen column density cases (Cassinelli et al. 1993).

The standing shock temperature is also too low to produce a significant X-ray flux at the K-shell edge of C and the K-shell and L-shell edges of Si (except at the highest rotation rates); therefore, the superionization seems to occur as a result of thermal ionization in the postshock material. At rotation rates just above the disk formation threshold, the shock temperature does coincide with the maximum abundance of C IV and Si IV (Shull & Van Steenberg 1982), and both are common wind diagnostics in Be star spectra. A plot of the frequency of Be stars that exhibit N V versus spectral type shows a strong cutoff at about B1 and N V is only rarely observed at later spectral types (see Fig. 1 of Marlborough & Peters 1982). At about this same spectral type, the terminal velocity in the wind is rapidly decreasing (see Fig. 4). This cutoff may, therefore, be due to the decrease in the strength of the wind instability shocks and at later spectral types N V will only be present if the disk shock is strong enough, that is, if the rotation rate is large enough. The maximum abundance for N V occurs at log $T = 5.3$; therefore,

we expect that N V should only be present if $V_{rot} > 400$ km s^{-1}. This might explain why, in later spectral types, N V is only rarely present in Be star spectra; whereas, C IV and Si IV are more common.

The shocks are adjacent to the disk; therefore, C IV and Si IV should be observed to be concentrated toward the equator. This agrees with observations of K. S. Bjorkman (1989) and Grady et al. (1987, 1989), who find statistical trends of the C IV properties with inclination angle and $v \sin i$ which indicate that C IV is concentrated toward low latitudes. As we explained in the Introduction, this has been quite puzzling. A primary reason for this belief is that no mechanism was known which could account for a high-velocity flow in the same latitudes as a low-velocity equatorial disk. Our model neatly explains this discrepancy in the following way: First, since the shock occurs at $r_{sh}^{min} < r < \infty$, and since the parallel velocity component is unaffected by the shock, C IV will be present at velocities up to the terminal velocity in the wind. Second, since the C IV is produced in the postshock region, the C IV will be enhanced at low latitudes. Third, the standing shock turns the high velocity flow to parallel the disk. This permits the existence of a high velocity component adjacent to the low-velocity disk (at essentially the same latitude since the disk is so thin).

It might seem that the disk could be accelerated to the same speed as the wind, since the material added to the disk will inevitably mix (due to viscosity). However, although the wind adds momentum to the disk, most of the material and momentum is added at small r before it has been accelerated to the terminal velocity of the wind (see Fig. 5, particularly the high rotation rate cases). The terminal speed that the disk obtains will then depend crucially on how the radiation forces are affected by the resulting increase in density. Because of this, we conclude that we may not rule out the possibility that the disk will remain at a slow speed, consistent with the Hα observations. There are several mechanisms which encourage us to believe that it may be possible that a model of the disk dynamics will predict a low-velocity disk. First, the radiation force term depends inversely on the density, so a high-density disk should be accelerated less than the polar wind; consequently, the disk will have a lower terminal velocity than the wind. Second, the shock is initially a strong shock which implies that the velocity in the disk is subsonic and will have to accelerate through a second critical point. Because of the velocity decrease, the material interior to the shock will "shadow" the disk, thereby reducing the radiative acceleration.

4.4. *Variability*

Our model is a steady state model, and we have made no attempts to explain the notorious variability of Be stars. Since the variability of Be stars is such an important facet of their behavior, we are compelled to examine our model for either sources that may induce variability, or phenomena arising from variability in the stellar mass-loss mechanism. We present our speculation concerning three such items here.

First, the disk location depends quite sensitively on the value of the terminal speed of the wind. From Figure 7, we see that for rotation rates just above the threshold rotation rate, a small change in the terminal speed, that is, a change in ζ, will cause a large change in the disk location, perhaps even causing the disk to disappear. Of course any change in the disk location will change the disk density and resulting observable phenomena. One prediction from this idea is that some Be stars would be more variable than others; in particular, those rotating at rates just above the disk formation threshold would be the most variable. Changes in the terminal speed might be brought about by changes in the ionization balance in the wind. An example of such a change is the bi-stability mechanism of Pauldrach & Puls (1990). If the change in ionization stage is like a phase transition (e.g., recombination of hydrogen when the optical depth becomes large in the bi-stability mechanism), the change in disk properties may be quite large and abrupt. A possible origin for changing ionization properties might be changes in the photospheric temperature associated with nonradial pulsations.

Second, we note that the shock that forms the disk is not attached to the star, but is instead free-standing. As such, the stability of its location depends on the shock velocity exactly balancing the flow velocity. It is not clear whether there is a feedback mechanism that regulates the shock strength to accomplish this balance. It is quite conceivable, therefore, that the shock location is in fact unstable. If so, perhaps the disk is actually made up of a series of shocks shed from the convergent point, that is, a "shock train." A similar phenomena is the latitudinal location of the disk, which is determined by balancing the ram pressure of the flow from the northern hemisphere with that from the southern. Perhaps the disk moves up and down in latitude in response to variations in the mass-loss rates between the two hemispheres.

Finally, we consider that perhaps there is an instability in the driving mechanism that occasionally causes blobs of material to be ejected. These blobs may subsequently move out through the wind and then enter the disk. Poe, Owocki, & Castor (1990) show that if the mass-loss rate in the supersonic portion of a wind is too large, then as the material flows outward, the velocity decreases back to the sonic value; subsequently, the material would presumably fall back onto the stellar surface. Suppose that occasionally enough material were ejected to "overload" the disk. At that time, the outflow in the disk would cease and the disk would collapse. This infall of the disk might then be used to explain the V/R variations seen in Be stars (see Dachs 1987). In a similar scenario, one might envision the possibility that only the inner portion of the disk is "overloaded," due to the addition of most of the material at small radii, and exhibits infall. On the other hand, the outer portion of the disk has only a small amount of material added to it, so it may flow outward. Thus there might be a stagnation point in the disk such that, interior to the stagnation point, the material recirculates back on to the star, and exterior to the stagnation point, there is outflow in the disk. In this scenario, changes in location of the stagnation point will change the relative amount of material flowing outward versus inward and perhaps might be the explanation of the V/R variations.

5. CONCLUSIONS

We have developed a model of the supersonic portion of the stellar wind from a rotating star. In the supersonic limit, the fluid equations are Newton's equations of motion for free particles. The orbital plane of each streamline is inclined with respect to the equatorial plane by the initial latitude of the streamline, thus orbital dynamics inevitably leads to an equatorial concentration of the wind. If the rotation rate is large enough, the orbits attempt to cross the equator, and a standing shock must develop to turn the flow. The ram pressure of the wind compresses and confines the equatorial material, and

creates a dense equatorial disk. We thus call our model the wind-compressed disk model.

Owing to the small ratio of the terminal velocity of the wind to the escape speed for B2 stars, the onset of disk formation occurs at a rotation speed of about 50% of breakup ($V_{rot} > 250$ km s^{-1}); whereas for early O stars, the disk can only occur for rotation speeds in excess of 90% of breakup. The theoretical values of the terminal speed of the wind qualitatively explains the frequency distribution of Be stars, and predicts a maximum likelihood near B2.

The disk is quite thin ($\Delta\theta \approx 0.^{\circ}5$) and has a density enhancement $\rho_{eq}/\rho_{pole} \approx 10^3$. In addition, the standing shock heats the boundary flow to temperatures 10^5–10^6 K before mixing with the disk. The shock cools radiatively by continuum recombination as well as line radiation with peak emission in the EUV and total luminosity $L_{EUV} \approx 10^{29}$ ergs s^{-1} $\approx 10^{-7.8} L_{bol}$. The shock temperature is inadequate to produce superionization by the Auger effect, but the temperature is large enough to collisionally ionize the shocked material. At this temperature the C IV and Si IV abundances are at their maximum. Since the shock temperature depends on the stellar rotation rate, we predict that highest observed stage of superionization *produced by the disk* should correlate with stellar rotation rate. Since the shock is adjacent to the disk, we also predict that the discrete absorption components of the superionized lines (such as C IV) will be concentrated toward low latitudes with more or less the same velocity structure, $v_r(r)$, as the polar wind.

The next task is to attempt to develop a model of the disk dynamics. An important theoretical test of our wind-compressed disk model will be whether the model of the disk dynamics permits a low-velocity disk that is consistent with the Hα observations. Finally, we would like to focus attention on what our model implies is the key element in forming an equatorial disk. To produce a disk at a reasonable rotation rate, our model required the observation that $v_\infty/v_{esc} \approx 1$ in the winds of Be stars.

We would like to thank K. S. Bjorkman, S. P. Owocki, J. S. Mathis, and L. S. Sparke for many useful discussions regarding this work. We would also like to thank the referee, J. M. Marlborough, for prompting us to more fully investigate the behavior of the disk formation threshold verses spectral type. This work was supported under NASA grant NAGW-422 and NASA contract NAS5-26777.

REFERENCES

Abbott, D. C. 1982, ApJ, 259, 282
Baade, D. 1984, A&A, 135, 101
Batchelor, G. K. 1967, An Introduction to Fluid Dynamics (Cambridge: Cambridge University Press), 135–136
Bjorkman, J. E., & Cassinelli, J. P. 1990, in Angular Momentum and Mass Loss for Hot Stars, ed. L. A. Willson & G. H. Bowen (Dordrecht: Kluwer), 185
Bjorkman, K. S. 1989, Ph.D. thesis, Univ. Colorado
Cassinelli, J. P., Cohen, D. H., MacFarlane, J. J., Sanders, W. T., & Welsh, B. Y. 1993, ApJ, submitted
Cassinelli, J. P., & Olson, G. L. 1979, ApJ, 229, 304
Cassinelli, J. P., Schulte-Ladbeck, R. E., Poe, C. H., & Abbott, M. 1989, in Physics of Luminous Blue Variables, ed. K. Davidson, A. F. J. Moffat, & H. J. G. L. M. Lamers (Dordrecht: Kluwer), 121
Castor, J. I., Abbott, D. C., & Klein, R. I. 1975, ApJ, 195, 157 (CAK)
Cayrel, R. 1963, C. R. Acad. Sci. Paris, 257, 3309
Coté, J., & Waters, L. B. F. M. 1987, A&A, 176, 93
Coyne, G. V., & McLean, I. S. 1982, in IAU Symp. 98, Be Stars, ed. M. Jaschek & H.-G. Groth (Dordrecht: Reidel), 77
Dachs, J. 1987, in IAU Colloq. 92, Physics of Be Stars, ed. A. Slettebak & T. P. Snow (Cambridge: Cambridge Univ. Press), 149
Doazan, V., et al. 1985, A&A, 152, 182
Drew, J. E. 1989, ApJS, 71, 267
Friend, D. B., & Abbott, D. C. 1986, ApJ, 311, 701 (FA)
Friend, D. B., & MacGregor, K. B. 1984, ApJ, 282, 591
Gehrz, R. D., Hackwell, J. A., & Jones, T. W. 1974, ApJ, 191, 675
Grady, C. A., Bjorkman, K. S., & Snow, T. P. 1987, ApJ, 320, 376
Grady, C. A., Bjorkman, K. S., Snow, T. P., Sonneborn, G., Shore, S. N., & Barker, P. K. 1989, ApJ, 339, 403
Hayes, D. S. 1978, in IAU Symp. 80, The H-R Diagram, ed. A. G. Davis Philip & D. S. Hayes (Dordrecht: Reidel), 65
Hearn, A. G. 1988, in Pulsations and Mass Loss in Stars, ed. R. Stalio & L. A. Willson (Dordrecht: Kluwer), 211
Howarth, I. D., & Prinja, R. K. 1989, ApJS, 69, 527
Kato, T. 1976, ApJS, 30, 397
Klein, R. I., & Castor, J. I. 1978, ApJ, 230, 902
Koninx, J.-P., & Hearn, A. G. 1991, in ESO Workshop on Rapid Variability of OB-Stars: Nature and Diagnostic Value, ed. D. Baade (Garching bei München: European Southern Observatory), 279
Krolik, J. H., & Raymond, J. C. 1985, ApJ, 298, 660
Kudritzki, R. P., & Hummer, D. G. 1990, ARA&A, 28, 303
Kudritzki, R. P., Hummer, D. G., Pauldrach, A. W. A., Puls, J., Najarro, F., & Imhoff, J. 1992, A&A. 257, 655
Kudritzki, R. P., Pauldrach, A., Puls, J., & Abbott, D. C. 1989, A&A, 219, 205
Lamers, H. J. G. L. M., & Pauldrach, A. W. A. 1991, A&A, 244, L5
MacFarlane, J. J., & Cassinelli, J. P. 1989, ApJ, 347, 1090
Marlborough, J. M., & Peters, G. J. 1982, in IAU Symp. 98, Be Stars, ed. M. Jaschek & H.-G. Groth (Dordrecht: Reidel), 387
Marlborough, J. M., Snow, T. P., & Slettebak, A. 1987, ApJ, 224, 157
Owocki, S. P., Castor, J. I., & Rybicki, G. B. 1988, ApJ, 335, 914
Owocki, S. P., & Rybicki, G. B. 1984, ApJ, 284, 337
Pauldrach, A. W. A. 1987, A&A, 183, 295
Pauldrach, A. W. A., Kudritzki, R. P., Puls, J., & Butler, K. 1990, A&A, 228, 125
Pauldrach, A. W. A., & Puls, J. 1990, A&A, 237, 409
Pauldrach, A. W. A., Puls, J., & Kudritzki, R. P. 1986, A&A, 164, 86
Pijpers, F. P., & Hearn, A. G. 1989, A&A, 209, 198
Poe, C. H. 1987, Ph.D. thesis, Univ. Wisconsin
Poe, C. H., & Friend, D. B. 1986, ApJ, 311, 317
Poe, C. H., Friend, D. B., & Cassinelli, J. P. 1989, ApJ, 337, 888
Poe, C. H., Owocki, S. P., & Castor, J. I. 1990, ApJ, 358, 199
Poeckert, R., & Marlborough, J. M. 1976, ApJ, 206, 182
Popper, D. M. 1980, ARA&A, 18, 115
Prinja, R. K., Barlow, M. J., & Howarth, I. D. 1990, ApJ, 361, 607
Schmidt, G. D. 1988, in Polarized Radiation of Circumstellar Origin, ed. G. V. Coyne, S. J., A. M. Magalhães, A. F. J. Moffat, R. E. Schulte-Ladbeck, S. Tapia, & D. T. Wickramasinghe (Tucson: Univ. Arizona Press), 641
Schulte-Ladbeck, R. E., & Zickgraf, F.-J. 1988, in Polarized Radiation of Circumstellar Origin, ed. G. V. Coyne, S. J., A. M. Magalhães, A. F. J. Moffat, R. E. Schulte-Ladbeck, S. Tapia, & D. T. Wickramasinghe (Tucson: Univ. Arizona Press), 583
Schutz, B. F. 1980, Geometrical Methods of Mathematical Physics (Cambridge: Cambridge Univ. Press), 59
Shull, J. M., & Van Steenberg, M. 1982, ApJS, 48, 95
Slettebak, A. 1982, ApJS, 50, 55
Snow, T. P. 1981, ApJ, 251, 139
———. 1982, ApJ, 253, L39
Taylor, A. R., Waters, L. B. F. M., Lamers, H. J. K. L. M., Persi, P., & Bjorkman, K. S. 1987, MNRAS, 228, 811
van den Heuvel, E. P. J., & Rappaport, S. 1987, in IAU Colloq. 92, Physics of Be Stars, ed. A. Slettebak & T. P. Snow (Cambridge: Cambridge Univ. Press), 291
Vogt, S. S., & Penrod, G. D. 1983, ApJ, 275, 661
Waters, L. B. F. M. 1986, A&A, 159, L1
———. 1989, in Proc. 23 ESLAB Symp. on Two Topics in X-Ray Astronomy, Vol. 1, X-Ray Binaries, ed. J. Hunt & B. Battrick (Paris: European Space Agency), 25
Waters, L. B. F. M., Coté, J., & Lamers, H. J. G. L. M. 1987, A&A, 185, 206
Waters, L. B. F. M., Taylor, A. R., van den Heuvel, E. P. J., Habets, G. M. H. J., & Persi, P. 1988, A&A, 198, 200
Weber, E. J., & Davis, L., Jr. 1967, ApJ, 148, 217
Zickgraf, F.-J., Wolf, B., Stahl, O., Leitherer, C., & Appenzeller, I. 1986, A&A, 163, 119